KfK 4105
Oktober 1986

A Study on Tritium Separation from LiPb by Permeation into Na or NaK and Cold Trapping

J. Reimann, S. Malang
Institut für Reaktorbauelemente

Kernforschungszentrum Karlsruhe

K E R N F O R S C H U N G S Z E N T R U M K A R L S R U H E
Institut für Reaktorbauelemente

KfK 4105

A Study on Tritium Separation from LiPb by Permeation into Na or NaK and Cold Trapping

J. Reimann and S. Malang

Kernforschungszentrum Karlsruhe GmbH, Karlsruhe

Kernforschungszentrum Karlsruhe GmbH
Postfach 3640, 7500 Karlsruhe 1

ISSN 0303-4003

A Study on Tritium Separation from LiPb by Permeation into Na or NaK and Cold Trapping

SUMMARY

The tritium separation and recovery method discussed in this report appears to be a very promising technique for a LiPb self cooled blanket where an intermediate loop is required for safety reasons anyway. This technique can be also of interest for a water cooled LiPb blanket if a tritium purification unit exists in the water loop.

Considerable work has been done on cold trapping of hydrogen from Na flows for the fast breeder technology. More work is needed in respect to fusion blanket applications, especially, on hydrogen removal from cold traps by thermal hydride decomposition.

This report summarizes the state of the art on the precipitation and decomposition processes and discusses practical experiences with cold traps. Some ideas on a fusion blanket cold trap are outlined and a research program covering the more fundamental aspects for the next future is proposed.

Studie über Tritium Abtrennung von LiPb durch Permeation in Na oder NaK und Ausscheidung in Kaltfallen

ZUSAMMENFASSUNG

Die in diesem Bericht behandelte Methode der Tritium Abtrennung und Wiedergewinnung scheint sehr günstig zu sein für ein selbstgekühltes LiPb Blanket mit einem, aus Sicherheitsgründen erforderlichen, Zwischenkreislauf. Diese Methode kann auch von Interesse sein für ein wassergekühltes LiPb-Blanket, falls eine Tritium-Reinigungs-Anlage im Wasserkreislauf existiert.

Im Bereich der Schnellbrüter-Technologie wurden umfangreiche Arbeiten zur Abscheidung von Wasserstoff mittels Kaltfallen aus Na-Strömen durchgeführt. Sehr viel mehr Untersuchungen sind jedoch erforderlich in bezug auf die speziellen Erfordernisse von Kernfusions-Blankets. Besonders lückenhaft ist der Kenntnisstand über die Wasserstoff-Wiedergewinnung aus den Kaltfallen durch thermische Zersetzung.

Dieser Bericht faßt den Stand des Wissens zusammen über die Vorgänge bei der Abscheidung und Zersetzung; praktische Erfahrungen mit Kaltfallen werden diskutiert. Vorschläge für eine Fusionsblanket-Kaltfalle werden erläutert, und ein Forschungsprogramm wird vorgeschlagen zur Lösung der mehr grundsätzlichen Probleme der näheren Zukunft.

Table of Content

		Page
SUMMARY		1
NOMENCLATURE		3
1.	Introduction	5
2.	Fundamental Aspects	9
2.1	The Na-H-System	9
2.2	Influence of Impurities	14
2.3	Comparison between Na-H and NaK-H	18
2.4	Precipitation and Decomposition	19
2.4.1	Precipitation	19
2.4.2	Decomposition	27
2.5	Isotopic Effects	35
3.	Experiences with Cold Traps and Improved Designs	38
4.	Considerations for Regenerative Cold Traps for Tritium Recovery	48
5.	Tritium Separation System for the NET Blanket	52
5.1	Tritium Separation in an Intermediate Sodium Loop	52
5.1.1	Tritium Concentration in Sodium	54
5.1.2	Tritium Permeation through the Intermediate Heat Exchanger Tubes	55
5.1.3	Double-Walled Heat Exchanger between Lithium-Lead and Water	58
5.1.4	Tritium Permeation Losses to the Cooling Water	58
5.2	Other Options	61
5.2.1	Use of NaK instead of Na in the Intermediate Loop	61
5.2.2	Tritium Separation in the Primary and Secondary Loop	62
5.2.3	Tritium Separation by Cold Trapping in a Water-Cooled LiPb-Blanket	67
6.	Research Work to be Done	74
6.1	General Aim	74
6.2	Investigation of Precipitation Kinetics	74
6.3	Analysis of Precipitates	77
6.4	Investigation of the Hydride Decomposition Kinetics	77
REFERENCES		80

NOMENCLATURE

A	surface of heat exchanger, permeation window
A'	deposition surface area
C	factor
D	diffusion coefficient
E	enthalpy
g	acceleration due to gravity
h	height
I	inventory
K	Sieverts constant
k	mass transfer coefficient
k_o	factor
k^*	rate constant
m	liquid metal mass
$\dot{m}$	liquid metal mass flow rate
$\dot{m}_H$	protium mass flow rate
$\dot{m}_T$	tritium mass flow rate
n	exponent
p	partial pressure
p_G	total pressure
$Perm$	permeability
R	gas constant
R'	concentration ratio
Re	Reynolds number
r_B	bubble radius
S_c	Schmidt number
Sh	Sherwood number
s	wall thickness
T	temperature
t	time
v	velocity
x	concentration
Δx	concentration difference
y	variable

Greek Symbols

β	mass transfer coefficient
ε	cold trap efficiency
μ	dynamic viscosity
ν	kinematic viscosity
ρ	density
σ	surface tension
τ	residence time

Subscripts

B	bulk
d	decomposition
E	equilibrium
e	end of trapping
f	final condition
H, H_2	protium
H_{2p}	hydrogen plateau
LiPb	lithium lead alloy
Na	sodium
NaK	sodium potassium alloy
O	oxygen
perm	permeation
pu	processing unit
T,T_2	tritium
w	wall

1. Introduction

The tritium processing systems have to be chosen such that the tritium inventory in the total blanket system (blanket, primary coolant loop, tritium processing systems) is small, the tritium losses to the environment are below a given value and that the costs are acceptable. Depending on the blanket design, various tritium separation methods were proposed for liquid metal breeders (see e.g. Watson /1/, Demo /2/, BCSS-IR /3/), using a counter current helium flow, vacuum pumping, cold trapping in a secondary Na loop, tritium permeation, gettering by metals and molten salt extraction. These techniques were used alone or in combination. In the BCSS-IR /3/, the last two methods were judged best for Li, whereas for a selfcooled LiPb blanket cold trapping in Na was recommended using vanadium as structural material. In the final BCSS report /4/ a one loop system and tritium separation by a counter current helium flow was regarded (see also Sze /5/).

For the water-cooled LiPb blanket proposed for NET (see e.g. Bioggio et. al. /6/), Pierini /7/ also discussed the tritium separation using a counter current helium flow. Due to the high permeation rate into the water coolant a purification unit is required; costs were assessed in the INTOR-study /8/ to 50 - 100 Mio $.

Tritium separation by means of permeation into a gas stream combined with catalytic oxidation was already proposed very early by Watson /1/. Recently, Buxbaum /9/ presented a closed concept for the design of a Zr-Pd permeation window. In /10/ this concept was applied for NET conditions and critical issues were discussed in more detail.

Tritium permeation into Na or NaK and tritium separation by cold trapping also was already included in Watson's report /1/. This method is especially interesting for self-cooled blanket concepts where the liquid metal in the primary loop and the water in the heat sink have to be decoupled in any case for safety reasons. Fig. 1 shows schematically such a blanket system. The Na or NaK can be used either in a secondary loop or in the gap of a double walled heat exchanger. There are two options for tritium separation:

1) All the tritium bred in the LiPb permeates into the Na or NaK system. Only one tritium processing unit is then required (cold trap with subsequent process steps) operated either with a bypass stream (secondary loop) or

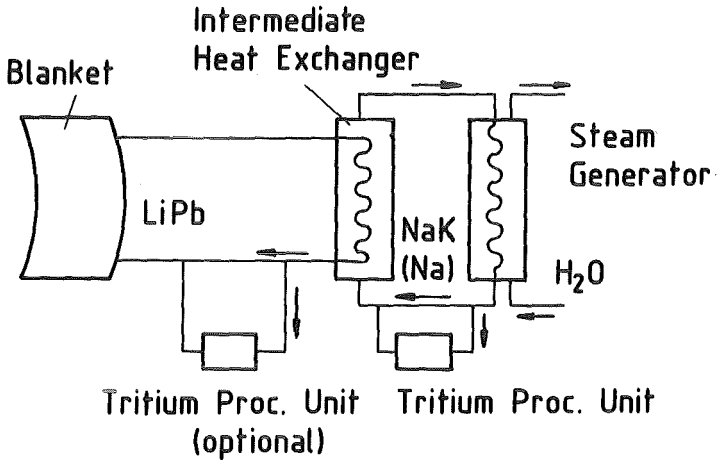

Self-Cooled LiPb Blanket with Secondary Loop

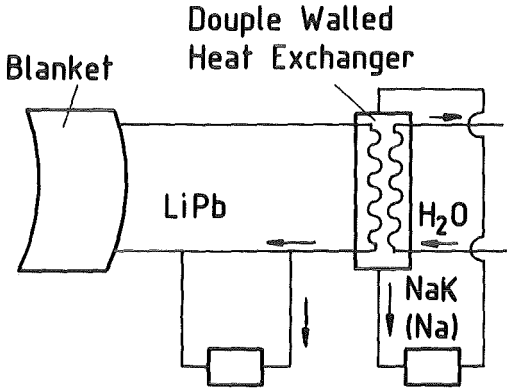

Self-Cooled LiPb Blanket with Double Walled Heat Exchanger

Fig. 1 Self-Cooled Blanket System

with the total gap flow rate. Both flow rates are typically in the order of some percents of the coolant flow rate of the secondary loop concept.

2) Most of the tritium is separated from the LiPb loop with an appropriate processing unit. The tritium which permeates into the Na or Nak must be separated with another processing unit to avoid the built up of a high tritium partial pressure which would result in an unacceptable tritium loss through the steam generator.

Both options were considered by Natesan and Smith /11/ for a self cooled Li blanket, in the present report these techniques are applied for a self cooled LiPb blanket for a NET reactor (Chapter 5).

The tritium separation by permeation of the total breed tritium into Na or NaK and cold trapping appears to be very promising for a self cooled LiPb blanket because the required area for the heat exchange is sufficient as permeation window if ferritic steels are used. Then the tritium processing unit in the LiPb loop is not required which facilitates the tritium flow sheet. However, this method can be also of interest for water cooled LiPb blankets if wall materials with a high tritium permeability have proven to be suitable as a permeation window.

The problems of LiPb in contact with wall materials with a high tritium permeability were discussed in the previous report /10/ and are not repeated here. If ferritic steels can be used these problems are much smaller, anyway. The compatibility of wall materials facing Na or NaK is much better and the chemistry of impurities in these liquid metals are much more understood. An important fact is that the oxygen affinity of Na or NaK is larger than the oxygen affinity of ferritic or austenitic steels. Therefore, oxygen in the Na or NaK system will not give rise to the built-up of permeation barriers at the wall surface. Therefore, this report concentrates on precipitating of tritium in and recovering from cold traps.

Cold traps have been used extensively to control impurity concentrations in sodium loops for fast breeder reactors because of their simplicity, economy of operation and effectiveness of achieving low impurity concentrations. The impurities of most concern are hydrogen and oxygen, which originate primarily from steam-generator corrosion, moisture from system-component surfaces, and

leakage of air into the system. High concentrations of these impurities in sodium can result in rapid corrosion of the system components or plugging of the flow passages or both. In addition to the corrosion and plugging problems, the background hydrogen concentration must be kept low to allow sensitive detection of steam leaks into the sodium.

The general experience in the past was that cold traps tended to plug when being loaded with a small percentage of the theoretical capacity (typically 10 %). This fact and the fact that the precipitating NaH masses were much larger than expected due to an unexpectedly high hydrogen permeation rate from the steam generator at the beginning of operation necessitated much more basic work to understand the fundamental processes and to develop codes for improved designs.

Previous work concentrated on the precipitation processes and only sparse work has been done in respect to regenerate cold traps that is to recover the hydrogen from cold traps.

In the following, fundamental aspects are discussed, the experience with current used cold traps is summarized and some ideas for a better design of cold tran for tritium separation and recovery are presented.

2. Fundamental Aspects

2.1 The Na-H-System

For most of the following discussions it is assumed that the solution mechanisms are equal for tritium (^3H), deuterium (^2H) or protium (^1H) atoms. Characteristical quantities such as the Sieverts constant and saturation concentration are then equal if these quantities are defined with the atomic fractions. Therefore, the term hydrogen is generally used if it has not to be differentiated in respect to the different isotopic masses. In experiments, mostly protium was used. Therefore, in literature the term hydrogen refers to protium. If the quantities are based on a weight fraction, the ratio of the molecular weights has to be taken into account if tritium is considered.

The main features of cold trapping can be explained by means of Fig. 2 which shows schematically the hydrogen partial pressure p_{H2} as a function of hydrogen concentration x for the system Na-H.
For low hydrogen concentrations (regime I), hydrogen is disolved as NaH in Na (characterized by index liquid). For dilute solutions the relationship between hydrogen concentration x and hydrogen partial pressure p_{H2} is represented by
Sieverts law:

$$x = K\sqrt{p_{H2}} \qquad (1)$$

where K is the Sieverts constant. Therefore, the Sieverts range is characterized by a straight curve if $p_{T2}^{0.5}$ is plotted versus x.

If the hydrogen concentration is increased at constant Na temperature the solution becomes saturated (saturation concentration x_{sat}): at higher concentrations (regime II) an additional solid NaH-phase (NaH_{solid}) coexists. This state is characterized by a plateau of the pressure curve (plateau pressure p_{H2p}). The discontinuity between the regimes I and II is well established for the NaH-system. For other systems this can be different (see Section 2.3).

At the end of regime II all the hydrogen exists as NaH_{solid}; in regime III, Na is dissolved in NaH_{solid}.

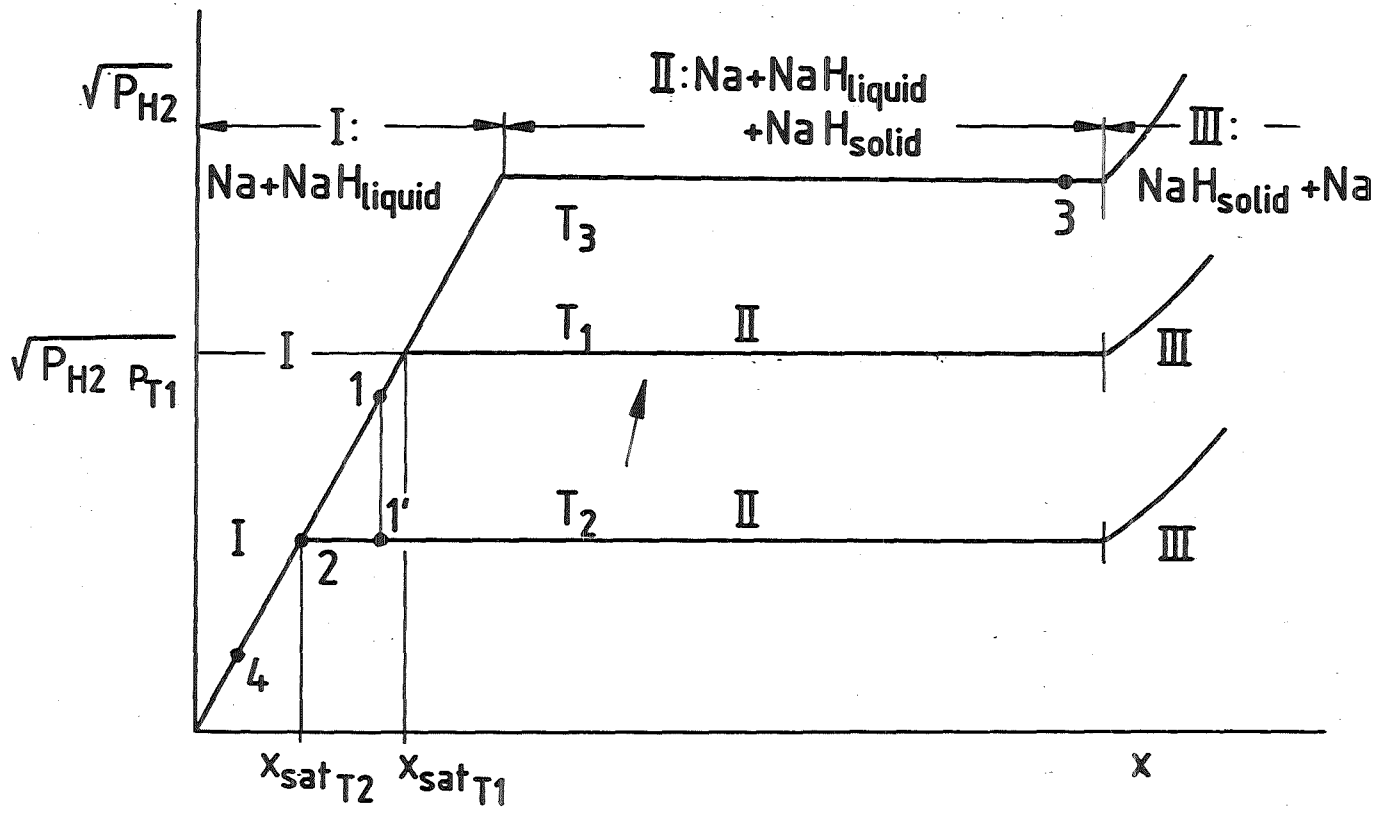

Fig. 2 Principle of Cold Trapping

The principle of hydrogen separation by cold trapping is as follows: When the liquid metal entering the cold trap with a temperature T_1 and concentration x_1 (Sieverts range) is cooled down to a temperature T_2, then the regime II is reached where NaH cristals are formed which precipitate in the cold trap. Ideally, the liquid metal leaves the cold trap with the concentration $x_{sat}(T_2)$, corresponding to the saturation concentration at the lowest temperature in the cold trap.

To recover the hydrogen, the cold trap is decoupled from the flow: the hydrogen concentration x_3 in the cold trap volume is high compared to x_1 (if the liquid metal is drained the concentration x_3 could be even in the ascending part of the curve). The system is heated up and the partial hydrogen pressure corresponding to point 4 is kept small by purging the system with an inert gas or by vacuum pumping. The solid NaH decomposes forming gaseous hydrogen and liquid Na: the hydrogen is collected outside of the cold trap. The hydrogen inventory in the residual liquid metal is neglectable if the equilibrium point 4 is reached.

In practice these equilibrium points 2 and 4 are not reached due to the limited time available for the mass transfer process. The precipitation and decomposition process are strongly dependent on the supersaturation, the residence time and other quantities which cause a thermodynamic unequilibrium.

For further discussions quantitative values are needed for the Sieverts constant K, the plateau pressure p_{H2p} and the saturation concentration x_{sat}. The temperature dependence of the Sieverts constant and is shown in Fig. 3 for different metals; the analytical relationships are given in Table 1. Most of the correlations were already used by Natesan and Smith; the values for LiPb-H were determined by Wu /12/, the correlations for Na-H and NaK-H (eutectic alloy with 78 weight % K) were recently recommended by Hubberstey /13/ summarizing previous work from Savage et al. /14/ and Ivanowich et al. /15/.

In the following it is often more convenient to use some quantities with units in wppm and Pa. (To remember: Na-H: 1 wppm = 23 appm, NaK-H: 1 wppm = 33,7 appm). For a relationship of the type

System	Equations	Ref.
Ti-H	ln K = 2.21 + 5390/T	11
Zr-H	ln K = 0.72 + 7540/T	11
V-H	ln K = 1.12 + 3490/T	11
Nb-H	ln K = 1.04 + 4280/T	11
Cr-H	ln K = 4.33 - 6330/T for T > 1050	11
	= -1.95 - 1940/T for T < 1050	11
Mo-H	ln K = 1.53 - 4420/T	11
Li-H	ln K = 1.32 + 6460/T	11
LiPb-H	ln K = -0.46	12
Na-H	ln K = 2.21	13
K-H	ln K = 3.91	13
NaK-H	ln K = 2.66 + 576*/T	13

* wrong sign given in /13/

Table I: Temperature Dependence of Sieverts Constant in Metal-Hydrogen Systems (K in appm/$\sqrt{Pa}$ and T in K)

$$\ln y = A - B/T \quad (K) \qquad (2)$$

the values given in Table II were recommended by Hubberstey /13/ for the constants A and B.

Fig. 4 shows the strong decrease of the hydrogen saturation concentration with temperature for some liquid metals; Fig. 5 the corresponding plateau pressures. The saturation concentration for Li is the highest which makes

	Na-H		NaK-H		K-H	
y	A	B	A	B	A	B
K(wppm/$\sqrt{Pa}$)	-0.921	-	-0,834	-576*	0.248	-
p_{H2p}(Pa)	31.82	14097	31.76	13723	31.12	13723
x_{sat}(wppm)	14.89	6961	15.06	6286	15.8	6862

* wrong sign given in Hubberstey's article

Table II: The Na-H and Na-K-System (from Hubberstey /13/)

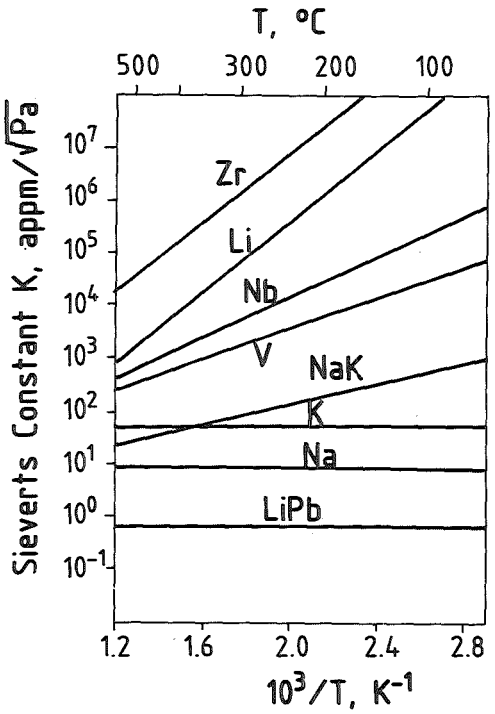

Fig. 3 Temperature Dependence of Sieverts Constant in Metal-Hydrogen Systems

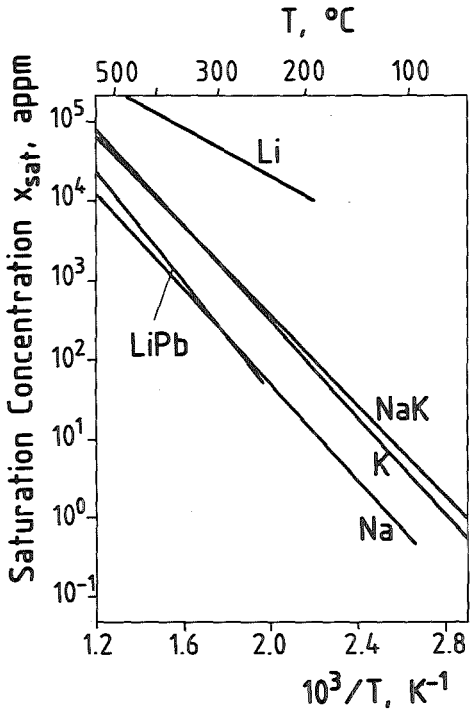

Fig. 4 Hydrogen Saturation Concentration

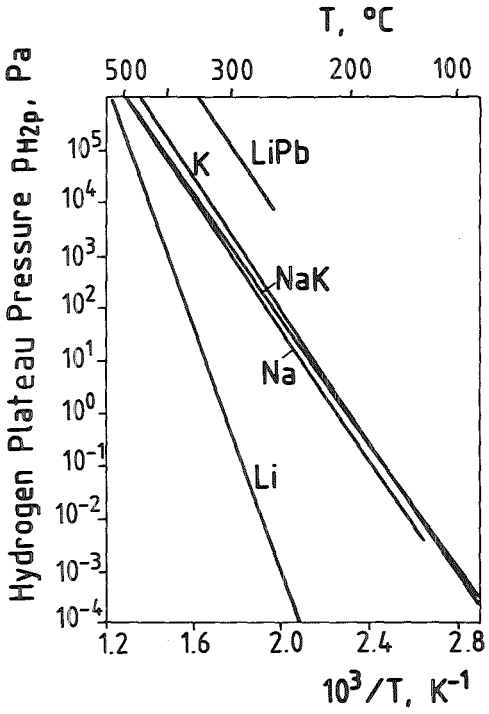

Fig. 5 Hydrogen Plateau Pressure

hydrogen separation by cold trapping very unfavourable. The values are not known yet for LiPb. A theoretical determination by Buxbaum /16/ results in values which, in combination with the high melting point (T_m = 235 °C), makes this method less attractive.

2.2 Influence of Impurities

Impurities in the system originate from impurities brought into the system in the start-up phase (impurities in delivered sodium, piping system) and impurities due to corrosion and small leaks from the heat exchanger when continuous operation is achieved. Of course the system has to be purified from the initial impurities prior starting the tritium processing. This could be done by an extra cold trap and eventually by an additional hot trap. An important aspect is the reduction of the oxygen concentration which determines the corrosion rate: typically a level in the ppm range is established in fast breeder liquid metal circuits.

The residual impurities can affect the tritium separation and recovery if tritium components are formed which

- precipitate outside the cold trap
- have a high solubility and do not precipitate at acceptable concentrations
- precipitate in the cold trap but are so stable that the tritium cannot be recovered.

Other components or elements have an adverse influence if they

- increase the solubility of hydrogen
- result in a high cold trap loading
- deteriorate the tritium recovery.

Typical impurities are oxygen, nitrogen, carbon and metallic corrosion products. Oxygen is the most important due the high chemical activity with sodium and the interaction with hydrogen. Fig. 6 (from Myles and Cafasso /17/) shows the phase diagram for the Na-H-O-System. Below 412 °C Na_2O and NaH coexist; with Na for relevant cold trap concentrations above 412 °C liquid NaOH is formed. Therefore, NaOH does not play any role during cold trapping; for cold trap regeneration, however, the formation and drainage of NaOH above 412 ° was proposed (see Section 3.3).

For dilute solutions (regime I in Fig. 2) the simultaneously dissolved oxygen increases the solubility of hydrogen. Fig. 7 (from Ullmann /18/) shows the

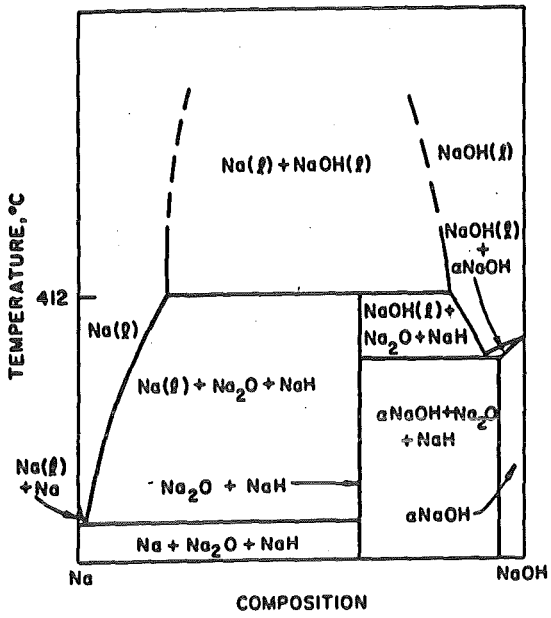

Fig. 6 Vertical Section Na-NaOH of the Na-Na_2O-NaOH-NaH System (from Mylos and Cafaso /17/)

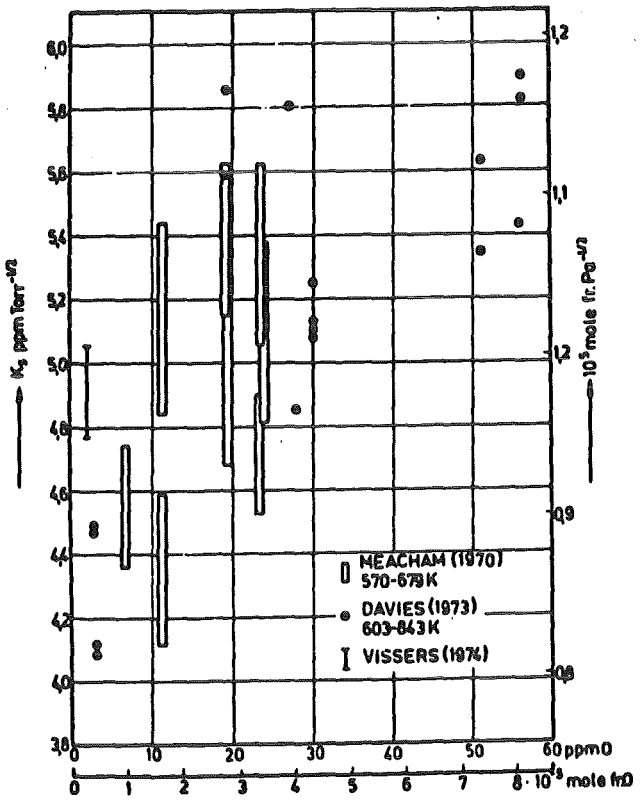

Fig. 7 Influence of Oxygen Dissolved in Sodium on the Sieverts' Constant (from Ullmann /18/)

increase of the Sieverts constant with increasing oxygen concentration which corresponds to a reduced hydrogen equilibrium pressure. In the application discussed here, the oxygen concentration is in the order of ppm and the effect on the Sieverts constant quite small.

The saturation solubility for Na_2O was determined by Noden /19/ to

$$\lg x_{sat\ O} = 0{,}415 - 2445/T \qquad (3)$$

with $x_{sat\ O}$ in mole fractions.

Fig. 8 shows a comparison of the saturation solubilities for NaH and Na_2O. Both curves are quite close; in practice often NaH and Na_2O simultaneously precipitate in the cold trap.
An important feature for the recovery of hydrogen is the fact that Na_2O is very stable and does not decompose if the system is heated up (pure Na_2O has a partial pressure of 10^{-10} Pa at 1000 K (Gmelin /20/). If the hydrogen is recovered at elevated temperatures (below 412 °C to avoid NaOH formation), Na_2O remains in the cold trap and accumulates with time.

In sodium loops the precipitation of various metallic impurities has been observed in the cold trap and at higher temperatures in the piping system. These precipitations often consist of ternary oxides such as chromites, silicates and ferrates (Grundy /21/). After precleaning the system these mass deposition rates in the cold trap should be small compared to the hydrogen deposition rate and therefore should not influence significantly the precipitation and recovery process. However, again the accumulation of these impurities contributions to the limited lifetime of the cold trap.

Nonmetallic impurities besides oxygen appear to be no problem because stable components are mostly formed only at high concentrations and temperatures, not relevant for the present application (Grundy /21/).

Some metals e.g. Li, Ba, Zr form more stable hydrides than Na (see e.g. Hobdell and Whittingham /22/). This fact is not significant for components made of ferritic or austenitic steel or vanadium.

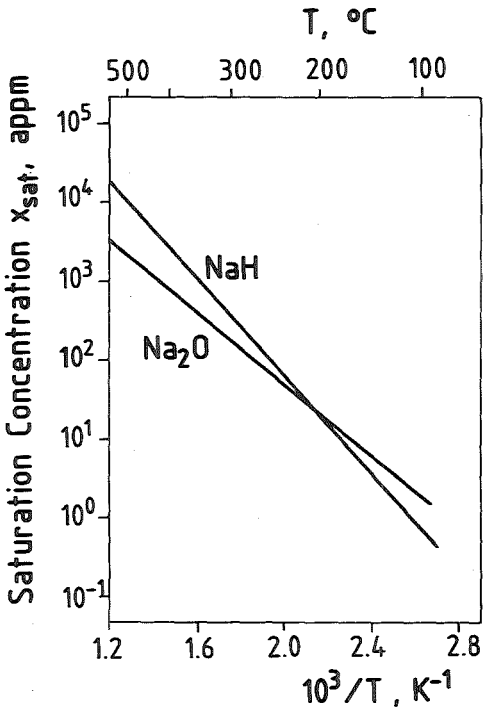

Fig. 8 Saturation Concentration of NaH and Na_2O in Na

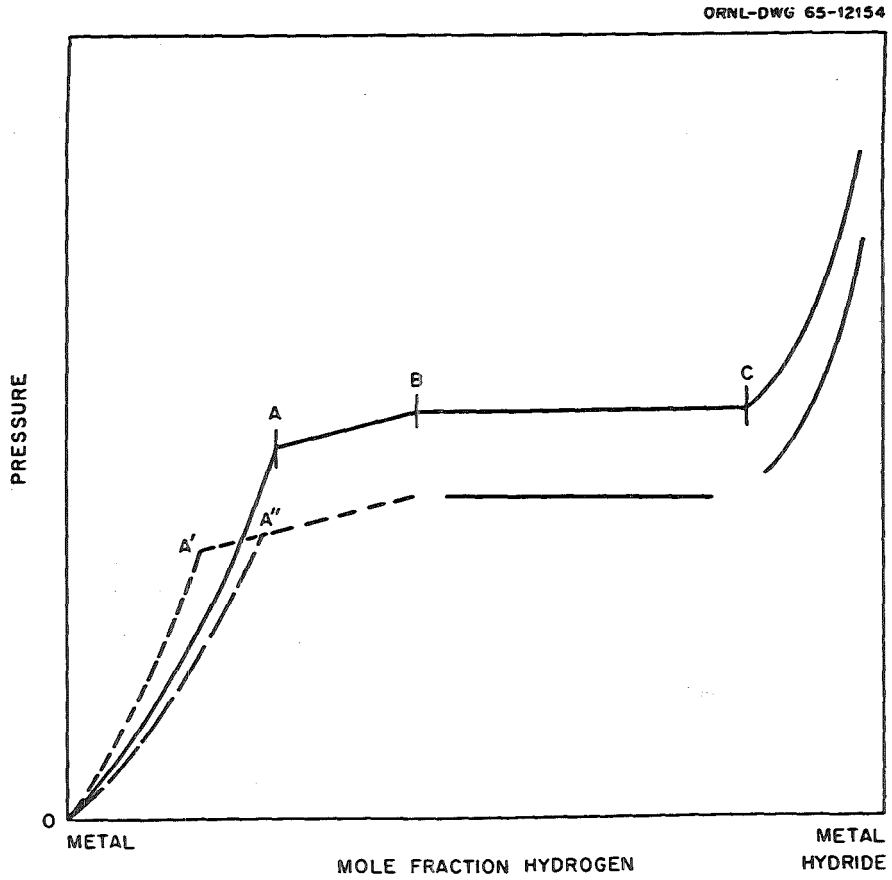

Fig. 9 Possible Isotherms in a Hydrogen-Alkali-Metal Mixture System (from Savage et. al. /14/)

2.3 Comparison between Na-H and NaK-H

The eutectic alloy NaK with 78 wt % K is very similar to Na in respect to several thermal properties. A distinct difference is the melting point of -12 °C for NaK compared to 98 °C for Na which favours NaK for many technical applications (no guard-heating system required). The low melting point makes NaK also attractive for cold trapping: For a cold trap temperature T_{CT} = 30 °C a hydrogen saturation concentration x_{sat} = 0,0034 wppm = 0,11 appm is calculated with Eq (2) whereas for Na-H and T_{CT} = 110 °C the value is x_{sat} = 0,038 wppm = 0,87 appm. However, the precipitation processes are expected to become much slower with decreasing cold trap temperatures T_{CT}. Therefore, the required residence time in the cold trap can be significantly larger to obtain the same cold trap efficiency.

The experiments from Savage et al. /14/ with NaK-H exhibited a disolution behaviour as shown in Fig. 2 (Sieverts law valid in regime I and p_{H2} = const in regime II). This was not expected by Savage et al. who assumed "that at point A (see Fig. 9) the precipitation of the solid hydride of a single metal begins. As precipitation continues in this system of mixed metals, the liquid composition will drift, as will plateau pressure, until a composition B is reached at which two metal hydrides begin to precipitate".

As mentioned, the NaK-H system behaves much more like a single metal-H system. However, no measurements exist on the composition of the precipitated hydrids, which is also of interest for the hydride decomposition process.

In general the knowledge on the NaK-H system is much more limited compared to the Na-H system. The results are based on experiments in a much more limited temperature range; the extrapolation to very low temperatures may give rise to considerable errors; more work is needed in this area.

An important criteria for the choice of NaK or Na in an intermediate loop according to Fig. 1 is the achievable partial pressure in the steam generator $p_{T2\ SG}$. The corresponding tritium concentration $x_{T\ SG}$ is given by

$$x_{T\ SG} = x_{T\ CT} + 10^6 \dot{m}_T / \dot{m}_{CT} \qquad (4)$$

where $\dot{m}_T$ is the tritium mass flow rate which has to be separated in the cold trap; and $\dot{m}_{CT}$ is the liquid metal mass flow rate into the cold trap. The concentrations have the dimensions wppm. The tritium concentration at the outlet of the cold trap $x_{T\ CT}$ is

$$x_{T\ CT} = 3 \cdot x_{H\ sat} \tag{5}$$

where $x_{H\ sat}$ is calculated with Eq (2) as function of the saturation temperature achieved in the cold trap. The tritium partial pressure $p_{T2\ SG}$ is given by

$$p_{T2\ SG} = (x_{T\ SG}/K_T)^2 \tag{6}$$

Again $K_t = 3 \cdot K_H$ and K_H is calculated with Eq (2) and Table II. Fig. 10 shows the tritium partial pressure $p_{T2\ SG}$ as a function of the saturation temperature which is for an ideal cold trap (efficiency = 1) equal to the minimum temperature in the cold trap T_{CT}; parameter is the cold trap mass flow rate $\dot{m}_{CT}$; the tritium mass flow rate is 50 g/d. A cold trap mass flow rate of $\dot{m}_{CT}$ = 5 kg/s corresponds to about 1 % of the required coolant mass flow rate in the intermediate loop. The use of NaK in combination with low cold trap temperatures results in considerably lower partial pressures compared to Na. Again it should be mentioned that these results were calculated assuming equilibrium (cold trap efficiency = 1); a more detailed discussion is given in Section 2.4.1.

The solution behavior of other elements (e.g. oxygen) is also less known in NaK compared to Na and experiments are required especially for low cold trap temperatures.

2.4 Precipitation and Decomposition

2.4.1 Precipitation

The processes governing the precipitation are crystal nucleation and cristal growth. These phenomena were described by Grundy /23/ as follows:
"For crystallization of solute from a solution to take place the solution must be supersaturated by some finite amount. This can be achieved by cooling the solution below the temperature corresponding to saturation solubility.

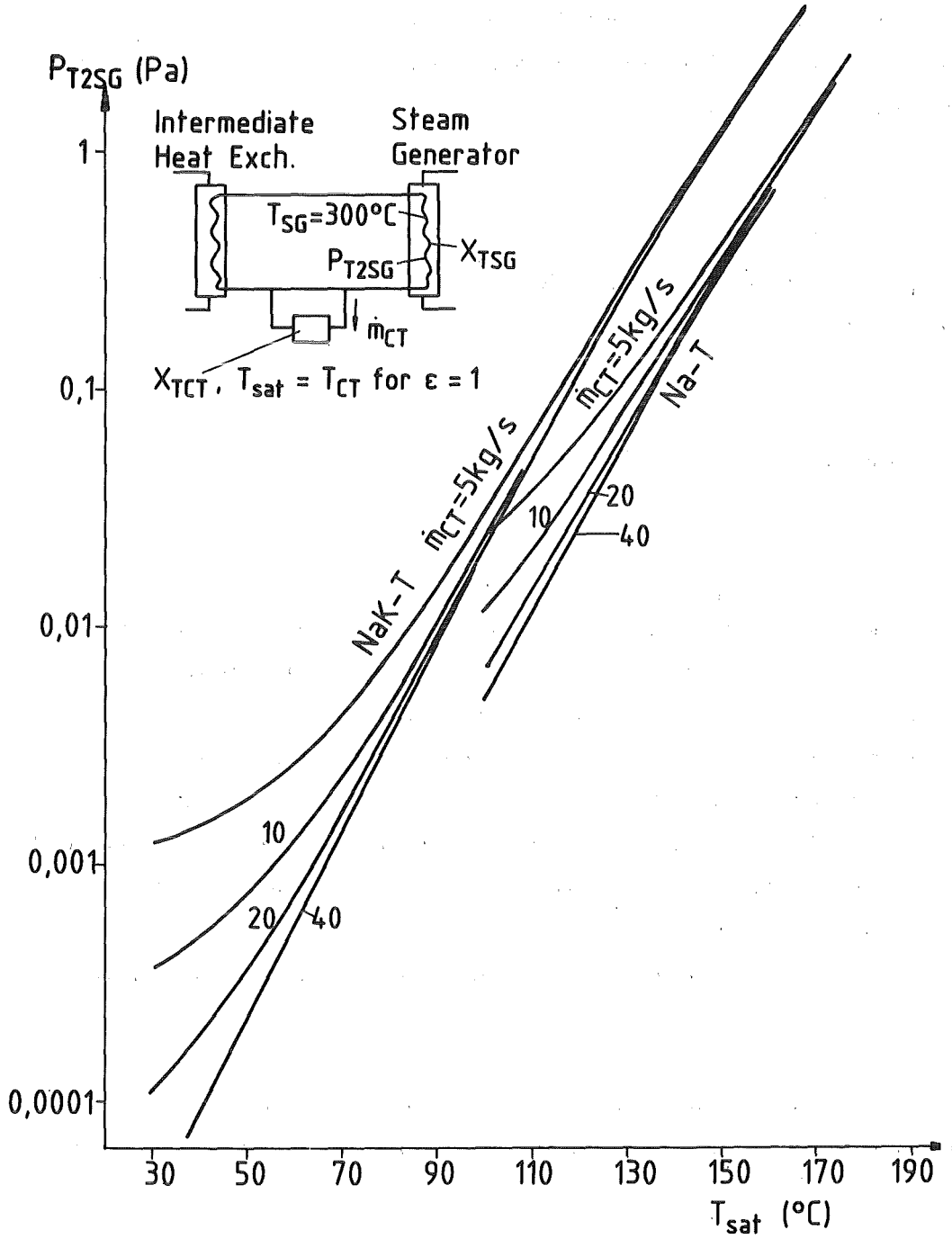

Fig. 10 Comparison between Na-T and NaK-T

Crystal growth rate is a linear function of supersaturation (when diffusion rate-controlled rather than reaction rate-controlled) whereas nucleation rate is an exponential function of supersaturation. At low supersaturation, rate of growth of existing crystals greatly exceeds nucleation rate, but at high supersaturation the converse could be true. Among the factors influencing degree of supersaturation required for nucleation are intensity of agitation of the solution, and the presence of foreign material which might form "seed" nuclei or provide active sites. Spontaneous nucleation in the liquid phase (homogeneous nucleation) usually requires higher supersaturation than nucleation on a foreign surface (heterogeneous nucleation). Then the preferred order of events as supercooling increases is, growth of existing crystals, heterogeneous nucleation, and finally homogeneous nucleation".

Presently, there are no measurement techniques to measure directly these processes in liquid metals. Valuable information is gained by measuring the cold trap inlet concentration x_{in} as a function of time, running the cold trap in a closed loop with a total mass of liquid metal m, a cold trap mass flow rate m_{CT} and starting the experiments with an inlet concentration x_o. The cold trap is ultimately capable of reducing the system impurity concentration x_{in}, to saturation solubility at the lowest temperature in the trap x_{sat}. The trap may not be able to achieve this concentration at its outlet in a single pass, only achieving a reduction to x_{CT}, where $x_{CT} > x_{sat}$. Definition of trap efficiency $\mathcal{E}$ provides recognition of this less than ideal behavior:

$$\mathcal{E} = (x_{in} - x_{CT})/(x_{in} - x_{sat}) \tag{7}$$

With the assumption of perfect mixing, the rate of reduction of impurity in the main system can be equated to the rate of removal by the cold trap:

$$- m(dx_{in}/dt) = \dot{m}_{CT}(x_{in}-x_{CT}) \tag{8}$$

Using Eqs (7) and (8) and solving the equation with the initital conditions $x_{in} = x_o$ for $t = 0$ gives

$$\ln((x_{in}-x_{sat})/(x_o-x_{sat})) = -\mathcal{E}(\dot{m}_{CT}/m)t \tag{9}$$

If $\mathcal{E}$ is constant and not a function of x_{in}, then the plots of ln fractional concentration against time should be linear, and the efficiency deducible from

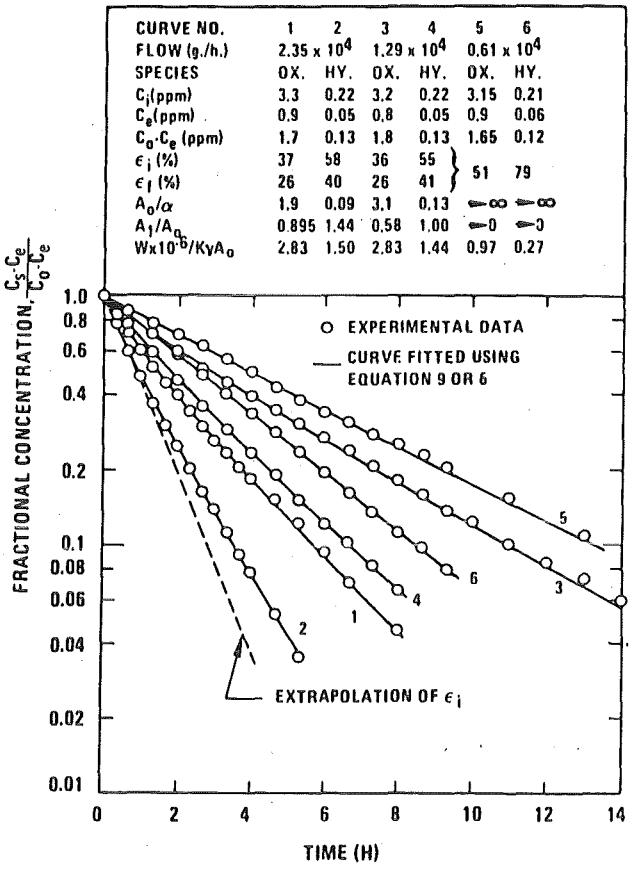

Fig. 11 Simultaneous Oxygen and Hydrogen Removal by the Packless Cold Trap (from Grundy /23/)

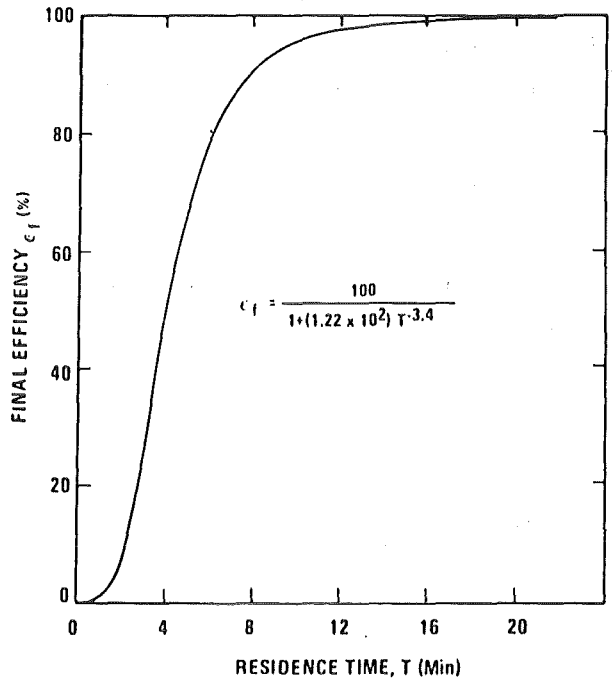

Fig. 12 Oxygen Trapping Efficiency of the Mesh-Filled Trap as a Function of Sodium Residence Time (from Grundy /23/)

the gradient. Figure 11 from Grundy /23/ shows such plots. Simultaneous removal of oxygen and hydrogen is shown for three sodium flowrates. Efficiency decreases as trapping proceeds but eventually reaches a constant value. Instantaneous efficiencies from the initial and final gradients ($\mathcal{E}_i$ and $\mathcal{E}_f$ respectively) are incorporated in the table included with Fig. 11.
The table also includes the initial steady-state concentrations (index i) and concentrations at the end of trapping (index e).

Fig. 12 (from Grundy /23/) shows results for the final efficiency $\mathcal{E}_f$ as a function of the residence time which is inversely proportional to the cold trap mass flow rate. This curve is not generally valid for the investigated cold trap but dependent on experimental conditions (inlet concentrations, cold trap loading). However, agreement exists with the generally accepted criteria to provide residence times of at least five minutes in order to obtain high cold trap efficiencies.

Feron /24/ performed similar experiments as shown in Fig. 11 but obtained typical discontinuities for the precipitation of NaH as shown in Fig. 13. The slope (efficiency) was fairly constant for each part of the curve. At the beginning of purification the supersaturation is large and nucleation and growth is expected to occur. At lower values of the supersaturation (right part of the curve) only growth of existing cristals occurs. Fig. 14 from /24/ contains results for the supersaturation where nucleation starts. For a cold trap temperature of 150 °C a supersaturation temperature of 12 °C is obtained for the cold trap with wire mesh. This is somewhat contradictory to the conclusions from McPheeters and Raue /25/ who pointed out that "significant supersaturation does not appear to occur before homogeneous nucleation begins when solid surfaces are available for nucleation sites, i.e., precipitation occurs on solid surfaces at all locations cooler than the saturation temperature".

This controversy again indicates that the results obtained are closely related to the specific experimental conditions and much more basic information is required to draw general conclusions.

To describe the cold trap behaviour in more detail models are required for the local nucleation and growth kinetics. Both processes were expressed by

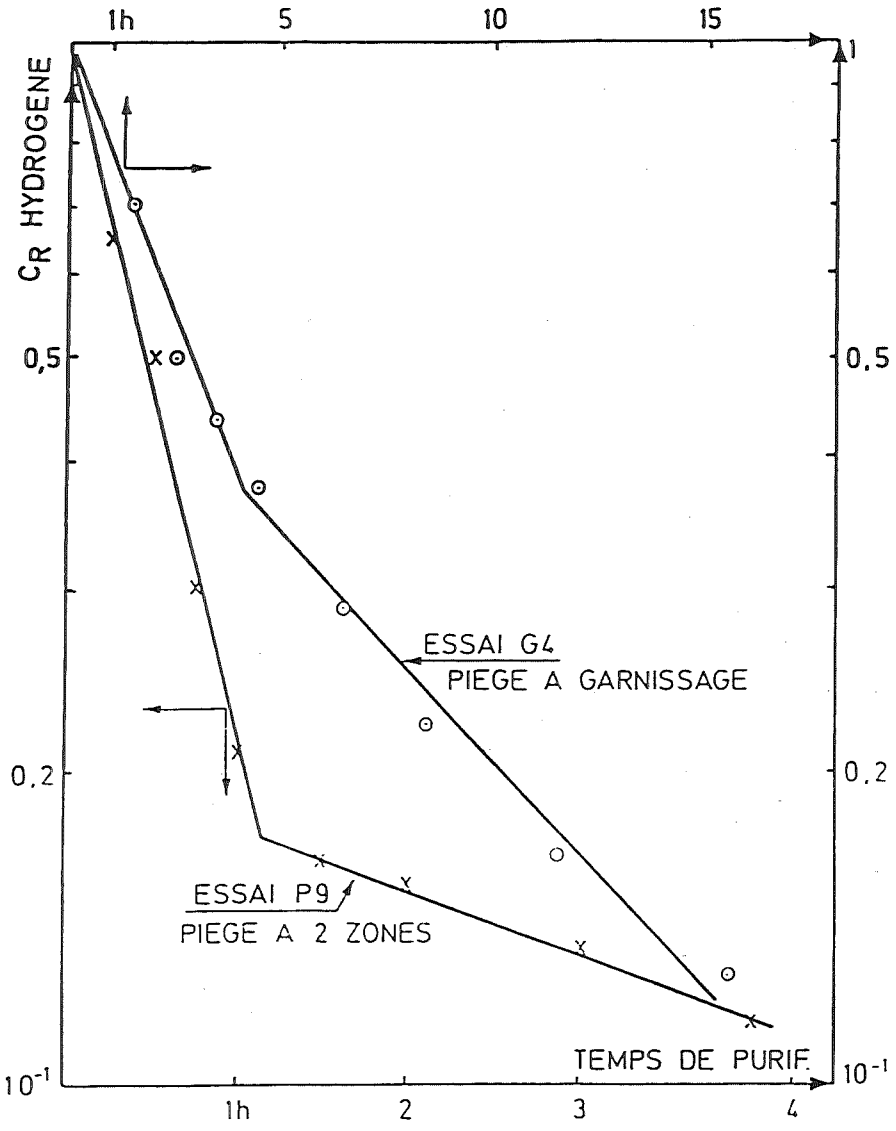

Fig. 13 Concentration C_R as a Function of the Purification Time (from Feron /24/)

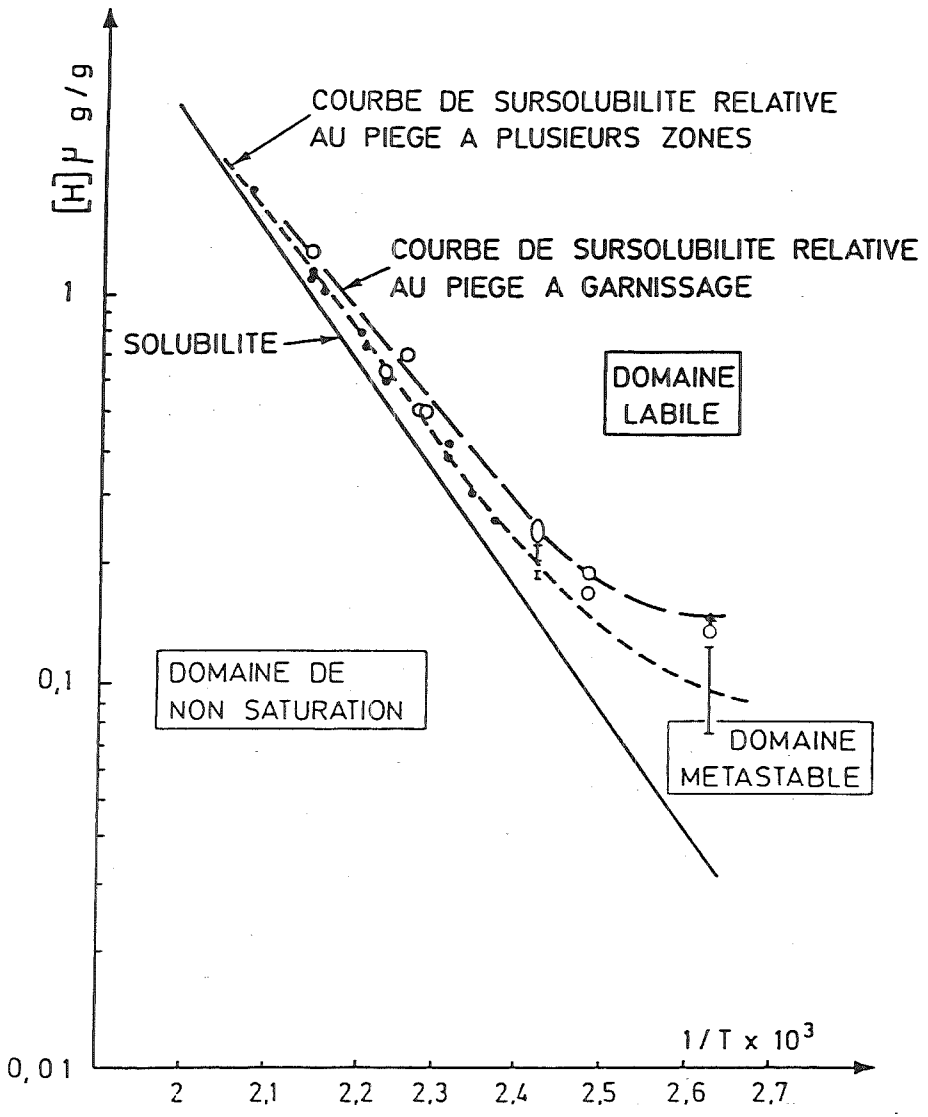

Fig. 14 Solubility and Supersaturation of Hydrogen in Sodium (from Feron /24/)

$$dm_H/dt = kA' \cdot (x - x_{sat})^n \qquad (10)$$

where m_H - mass of e.g. hydrogen in the deposit, kg
t - time, s
k - mass-transfer coefficient, m/s
A' - deposition surface area, m^2
x - local hydrogen concentration in the liquid metal, kg/m^3
x_{sat} - saturation hydrogen concentration in sodium based on the local temperature, kg/m^3
n - exponent indicating the order of the process

The growth rate is generally considered to be limited by diffusion. The exponent n is then assumed to be unity.

There are various correlations for the mass transfer coefficients; Latge /26/ used the following expression

$$k = k_o \cdot \exp(-E/RT) \qquad (11)$$

where k_o and E were determined experimentally for both nucleation and crystal growth.

Hebditch /27/ used correlations of the type

$$Sh = k \cdot d/D = f(Re, Sc) \qquad (12)$$

where Sh = Sherwood Number, Re = Reynolds Number, Sc = Schmidt Number, d = characteristical length, D = diffusion coefficient for hydrogen in sodium ($D = 6 \cdot 10^{-9}$ m^2/s for T = 200 °C).

McPheeters and Raue /25/ pointed out that attempts to correlate their results with an expression according to Eq. (5) were unfruitful. Their value of $k = 6 \cdot 10^{-5}$ m/s compares well with values of $4 \cdot 10^{-5}$ to 10^{-4} m/s estimated by Hebditch /27/ for a similar system.
The initial deposition surface area is the surface of the container and the packing. During cristal growth this area increases as shown in Fig. 15 (from /25/), where f is the dimensionless area factor which is a function of the quantity NaH deposited per unit area.

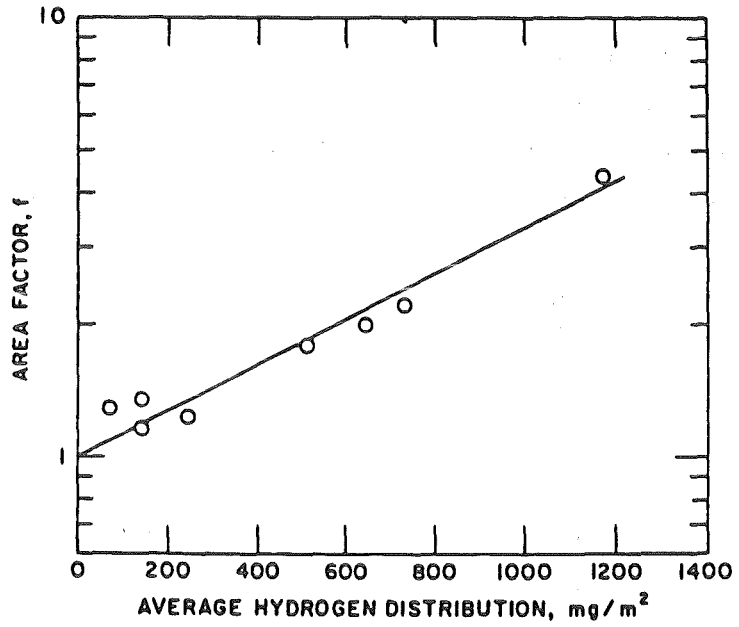

Fig. 15 Effect of NaH Deposition on the Surface Area Available for Precipitation (from McPheeters and Raue /25/)

An increase in effective surface area by a factor of four, as observed in these experiments, could have been achieved in any one of several ways. For example, if the NaH precipitated as small cubic crystals, the factor-of-four increase in surface area would occur if 10^9 crystals of 25 µm size precipitated per square meter of surface. It is more likely, however, that fewer crystals nucleated and that the growth was more needle-like or dendritic, as is the nature of NaH crystals. This open structure could have easily achieved a fourfold increase over the bare stainless steel area.

Latgé /26/ showed that the growth was regular when there was only a slight supersaturation. Otherwise dendritic formations were observed; in this case a surface crust rapidly obstructed the cold trap.

The models for local cristal nucleation and growth are implemented in computer codes to predict the behaviour of existing cold traps or to serve as an design tool for improved cold traps. One example for such a code is the MASCOT code developed by McPheeters and Raue /28/.

This two-dimensional code can simulate most configurations of packing materials and dimensions: it calculates first the flow distribution and pressure drop, then the temperature distribution and finally the impurity concentration profile, and impurity mass distribution. The rate of mass deposition is calculated with Eq. (10), assuming a first order reaction (n=1). The mass transfer coefficient k is determined from a Schmidt number correlation, nucleation times and cristal growth within the sodium are not taken into account. Comparisons between MASCOT and experiment will be presented in Section 3.

2.4.2 Decomposition

Compared to precipitation, work on hydrogen recovery from the cold trap is marginal. The recovery is usually accomplished by thermal decomposition of sodium hydride which has a hydrogen dissociation pressure 10^3 times greater than the vapor pressure of sodium. The hydrogen can therefore be removed either under vacuum or by purging/sparging with an inert gas when the trap is filled or drained of sodium.
Fidler and Whittingham /29/, pointed out that it is necessary to distinguish between hydrogen evolution in the presence or absence of bubble formation. For regeneration techniques involving an inert gas, when bubble formation does not occur because the total pressure is higher than the saturation pressure the degassing of liquid sodium can be summarised by the following equations:

$$\mathrm{NaH_{solid}} \xrightarrow{(i)} \mathrm{H_{solution}} \xrightarrow{(ii),(iii)}$$

$$\mathrm{2H_{surface}} \xrightarrow{(iv)} \mathrm{H_2} \xrightarrow{(v)} \mathrm{H_2\ (gas)} \qquad (13)$$

Steps (ii) and (iii) involve the diffusion of dissolved hydrogen to the liquid/gas interface and its transition from the absorbed to the adsorbed state at the surface. In principle the rate determining step can be determined from

the order of reaction.

However, Gwyther and Whittingham /30/ showed that heterogeneous nucleation and growth of hydrogen bubbles contributed significantly to H_2 evolution under vacuum, accounting for the greater rates observed under vacuum than under argon at normal pressure.

Bubble nucleation requires the gas equilibrium pressure p_E, corresponding to the solute concentration in the liquid metal to exceed the sum of the external pressure above the melt p_G, the hydrostatic pressure of any liquid sodium $g(h+r_B)\varsigma$, and the effect of surface tension σ, on the bubble, i.e.:

$$p_E > p_G + (h+r_B)\varsigma g + 2\sigma/r_B \qquad (14)$$

Here, r_B = bubble radius, g = acceleration due to gravity, h and ς are the height and density of liquid Na.
The critical radius for bubble nucleation occurs when $dP_E/dr_B = 0$ from which it can be shown (Winkler and Bakish /31/) that the minimum P_E for nucleation is $(8\varsigma\sigma g)^{1/2}$. This pressure corresponds to a temperature for equilibrium in the Na-H-O-system of 250 °C, below which no bubble formation occurs under vacuum.
The mechanism for heterogeneous bubble nucleation could involve the following steps:

$$NaH_{solid} \xrightarrow{\text{decomposition}} H_{atoms} \xrightarrow[\text{desorption}]{\text{diffusion}} \qquad (15)$$

$$H_{\text{bubble/metal interface}} \xrightarrow[\text{recombination}]{} H_2 \text{ (gas in bubble)}$$

After nucleation bubble growth occurs by continuous H_2 transfer from decomposing NaH particles and by expansion on rising through the liquid metal. Bubble coalescence results when the nucleation frequency is high as observed in practice. Under these conditions, the diffusion and recombination/desorption steps will be rapid and not rate limiting. Two other rate limiting steps involving NaH particles then require consideration.

If nucleation and growth on suspended particles is the slowest step, a first order rate equation is derived by assuming an equal probability for nuclea-

tion at each active site. Then the decomposition rate will be proportional to the mass of NaH particles.

$$dm_H/dt = k^* m_H \qquad (16)$$

where $k^* = s^{-1}$ is the rate constant.

Alternatively, if NaH decomposition is the slow step, the rate will be proportional to the surface area, A', of the particles. For spherical particles, A' is proportional to $m^{2/3}$ so that different orders of reaction (1 and 2/3) are predicted for the two mechanisms".

The few experiments available in literature are summarized in Table III: In the small scale experiments the NaH or Na_2O precipitates were simulated by NaH or Na_2O granulate; information on the specific surface area is only given in /29/. Typical vessel dimensions were 50 mm inner diameter and 150 mm in height. In experiments to simulate the sodium drained cold trap, the mixtures were suspended in stainless steel mesh above the bottom of the vessel. The mesh allowed liquid sodium produced by NaH decomposition to drain from the reactants.

Author	Small Scale Exp. (NaH granulate)				Intermediate Scale Exp. (NaH precipitate)		
	drained		undrained		drained		undrained
	vac. pump.	argon purge	vac. pump.	argon purge	vac. pump.	argon purge	vac pump.
Gwyther & Whittingham /30/			x	x			
Mc Pheeter & Raue /33/			x(1)	x			
Fidler & Whittingham /29/	x(1)		x(1)		x	x	x

(1) influence of Na_2O investigated

Table III: Hydrogen Decomposition Experiments

For the intermediate scale experiments a 100 l cold trap was used, the cold trap was loaded by NaH precipitation. Therefore, the cristallization morphology described in detail by Fidler et al. /32/, was more relevant than for the small scale experiments. Due to the small number of experiments under different conditions (e.g. three complete experimental runs with the intermediate scale cold trap) the results only allow to draw general conclusions.

If an inert gas purge (argon) was used the flow was always directed over the sodium surface and was not bubbled through the liquid sodium.

The experiments from Gwyther and Whittingham /30/ showed that heterogeneous nucleation and growth of hydrogen bubbles contributed significantly to H_2 evolution under vacuum, therefore, greater rates were observed under vacuum than under argon at normal pressure. In contrast to the work discussed in the following, only a small fraction of the hydrogen present initially as NaH was removed.

Fig. 16 presents typical results for the small scale experiments from Fidler and Whittingham /29/: The H_2 flow rate is shown as function of time including the temperature variation during regeneration.

The following observations were made /29/: "In all experiments where excess sodium was not present initially, the temperature fell by as much as 10 ^{o}C during the early stages of regeneration. This was followed by a gradual rise in temperature as thermal equilibrium between the furnace and the vessel contents was restored. This effect was due to the endothermic decomposition of NaH (60 kJ/mole) and it was therefore necessary to assign an average temperature for regeneration in these cases.

All regenerations were characterized by an initial rapid decrease in H_2 evolution rate, typically for the first few minutes of the reaction. This was followed by a slower but continuous fall in rate for the remainder of the process. The total H_2 recovered varied from 95 to 106 % of the initial amount, suggesting that essentially complete H_2 recovery was achieved even allowing for the possibility of a small amount of residual hydrogen dissolved in the sodium after regeneration.

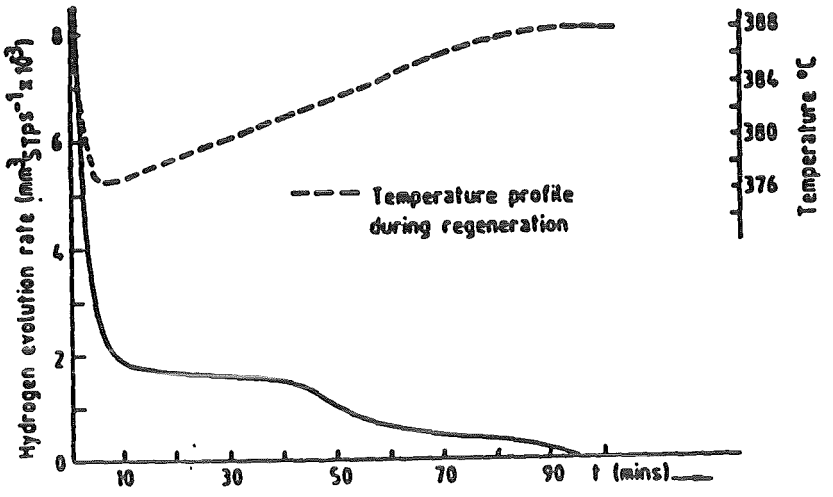

Fig. 16 Typical curve for H_2 evolution rate as a function of time for a NaH/Na_2O mixture (from Fidler and Whittingham /29/)

Visual observation of NaH decomposing initially in the absence of liquid sodium demonstrated that shortly after regeneration started, a liquid film formed. Small bubbles of H_2, <1 mm diameter, could be seen coming from the sodium surface which eventually formed a continuous film enveloping the NaH particles.

After the first few minutes of regeneration, the rate of H_2 evolution was proportional to the amount of hydrogen remaining in the mixture, i.e. the results apparently obeyed a first order rate law. This was somewhat surprising when appreciable temperature drops were observed because there is a marked temperature dependence of H_2 evolution rate and because more than one evolution mechanism may exist. Thus, while 'pseudo' first order rate constants can sensibly be used for comparing rates for different mixtures at a given temperature, it should not be assumed that the rate law describes a unique evolution mechanism."

Fig. 17 shows the results obtained by McPheeters et al. /33/ simulating an

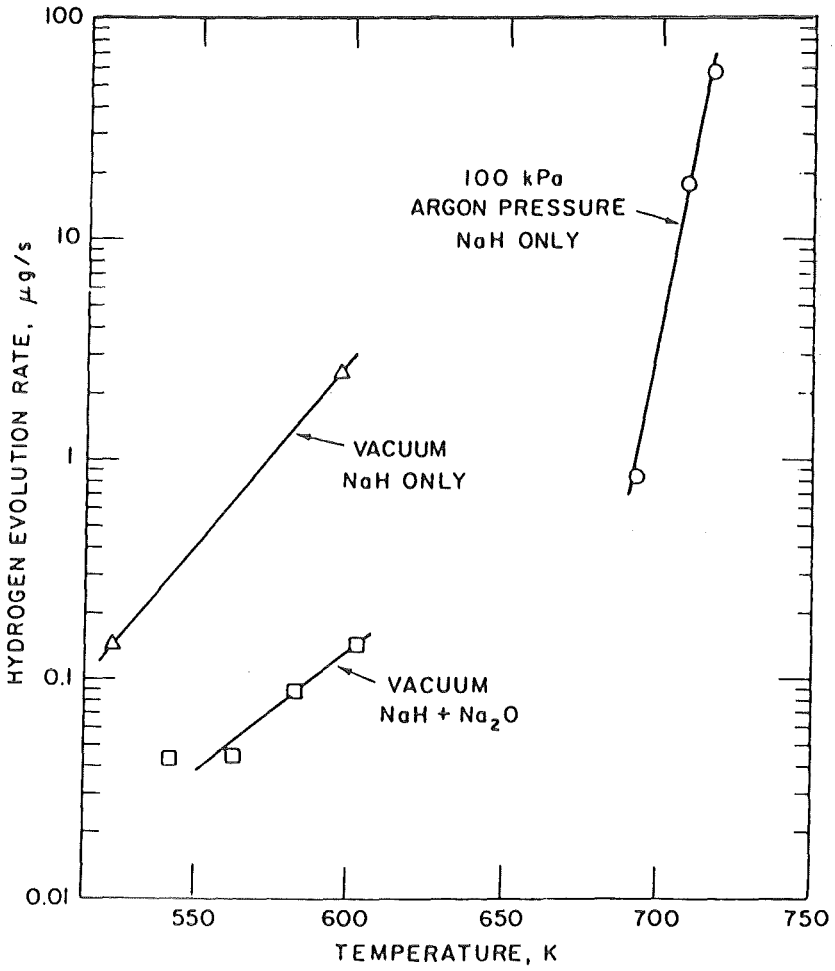

Fig. 17 Hydrogen Evolution Rates Observed in the Experiments (from McPheeters et. al. /33/)

undrained cold trap. A significantly higher temperature is needed to evolve hydrogen at atmospheric pressure than under vacuum. This observation is consistent with the theory that the primary mechanism for rapid hydrogen evolution is by bubble nucleation, growth, and release. The temperature difference between hydrogen evolution at 3 µg/s under atmospheric pressure and the same rate under vacuum was found to be 100 K. This temperature difference corresponds to a critical bubble radius of between 50 and 100 µm.

In these experiments the presence of Na_2O appeared to inhibit the hydrogen evolution rate by as much as one order of magnitude. This is in contrast to later results and to the results from Fidler and Whittingham /29/ where it was clearly pointed out that solid Na_2O has no inhibiting effect. In the presence of solid Na_2O, the plateau pressure in the Na-H-O-system is reduced relative to that in the Na-H system above 360 °C due to the reaction of hydrogen with solid sodium monoxide. However, Fig. /18/ (from /29/) shows that the driving force for bubble nucleation and growth is still high in the Na-H-O-system and the apparent absence of any inhibiting effect of Na_2O suggests that bubble nucleation and growth is the dominant mechanism for H_2 evolution whether or not Na_2O is present.

Fig. 19 (from /29/) compares results from different experiments. The rate constants k derived from regenerating fine NaH are appreciably greater than those from the coarse batch at corresponding temperatures. Vacuum regeneration was always more rapid and effective than argon purging. The results for the intermediate scale tests agree within an order of magnitude with the results for coarse NaH. This is considered quite acceptable for kg quantities of NaH some 50 times greater than those used in the small scale experiments. The lower rates in the intermediate cold trap can be attributed to the measured particle size being 100 µm which is coarser than in the small scale experiments. As stated in /29/, McPheeters et al. also found that the rate constants in intermediate scale vacuum regeneration ($\leq$800 g NaH) were up to an order of magnitude less than in small scale experiments.

Time scales for in-situ regeneration of LMFBR cold traps are estimated to be acceptable at the rates shown in Fig. 19 but in view of the particle size effect on H_2 evolution rates, comparisons between different experimental conditions are likely to be complicated by the form of the NaH deposit which may, for example, be very dense in the absence of a cold trap mesh.

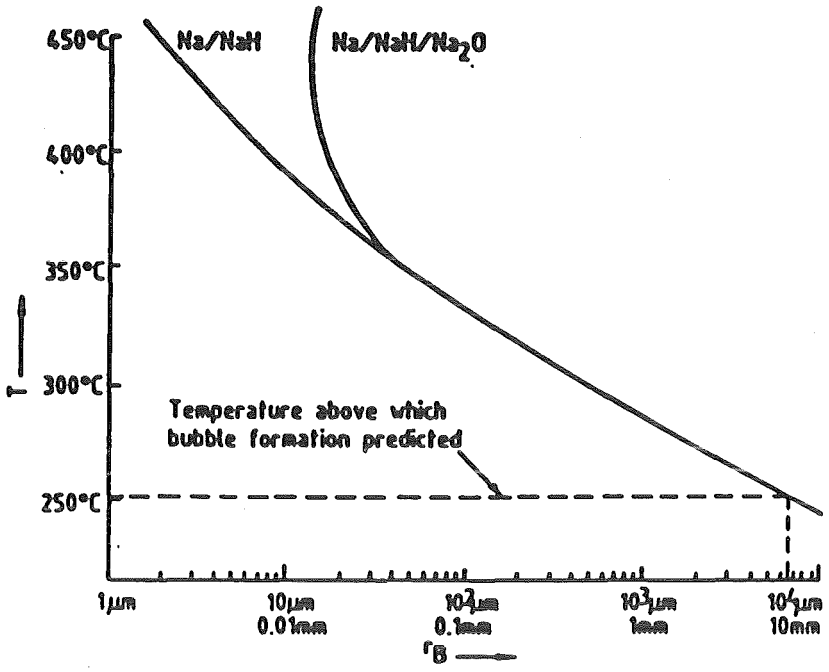

Fig. 18 Critical Bubble Radius as a Function of the Temperature of NaH-Saturated Sodium under Vacuum according to Fidler and Whittingham /29/

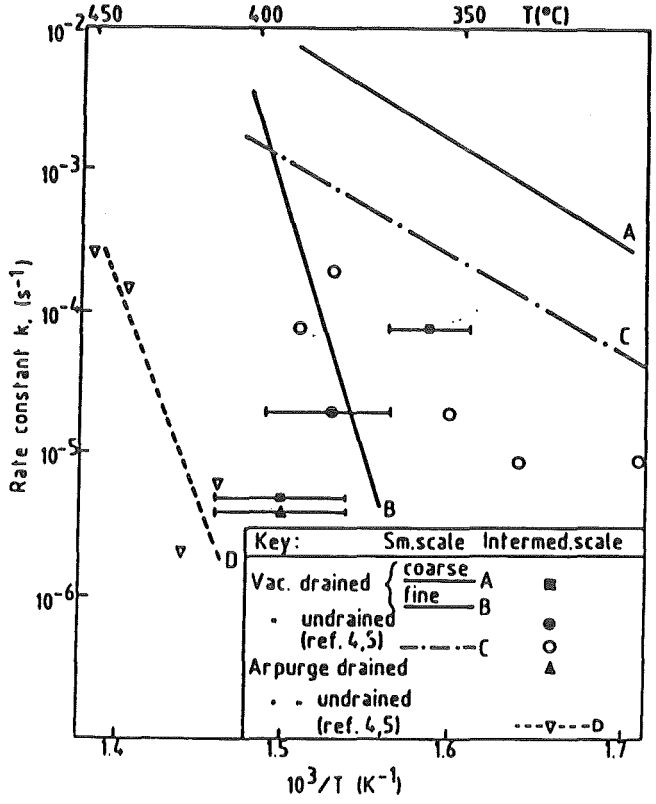

Fig. 19 Rate Constants as a Function of Reciprocal Temperature in Small and Intermediate Scale Regenerations (from Fidler and Whittingham /29/)

The extrapolation of these results for an optimized regenerative cold trap for tritium recovery is very difficult, much more basic experiments are needed in this area.

2.5 Isotopic Effects

Up to now the assumption was made that the solution mechanisms are independent on isotopic effects. This implies that tritium atoms precipitate with protium atoms in the same ratio as they exist in solution. This assumption was fairly well experimentally verified by McPheeters and Raue /34/. This coprecipitation can be purposely used to decrease the tritium by adding other hydrogen isotopes (e.g. protium) to the tritium (isotope swamping). For a given cold trap temperature the cold trap concentration (in appm) of the sum of the hydrogen isotopes (e.g. tritium (Index T) and protium (Index H)) is constant

$$x_{CT} = x_{T\ CT} + x_{H\ CT} = x_{T\ CT}(1+R') = \text{const} \qquad (17)$$

with

$$R' = x_H/x_T = (M_T/M_H)(\dot{m}_H/\dot{m}_T) \qquad (18)$$

where M is the molecular weight.

Fig. 20 shows the effect of the additional protium flow rate on the tritium partial pressure at the steam generator for the example already discussed in Chapter 2.3. For a given value of $p_{T2\ SG}$, isotope swamping decreases the required cold trap mass flow rate and increases the cold trap temperature. For a hydrogen isotopes mixture of 9 parts protium and 1 part tritium (mass ratio $m_H/m_T = 3/1$), the achievable tritium outlet concentration is 1/10 of that for tritium alone. If the tritium outlet concentration is kept constant, the additional protium allows higher cold trap temperatures; e. g. $T_{CT} \approx 172\ ^oC$, instead of 115 ^oC for Na.

Protium can be purposely added; on the other hand protium also permeates from the steam generator into the intermediate loop. The price to be paid for the isotopic swamping effect is the higher capacity of the final isotope separation unit (e.g. cryogenic distillation). This unit is required anyway for the

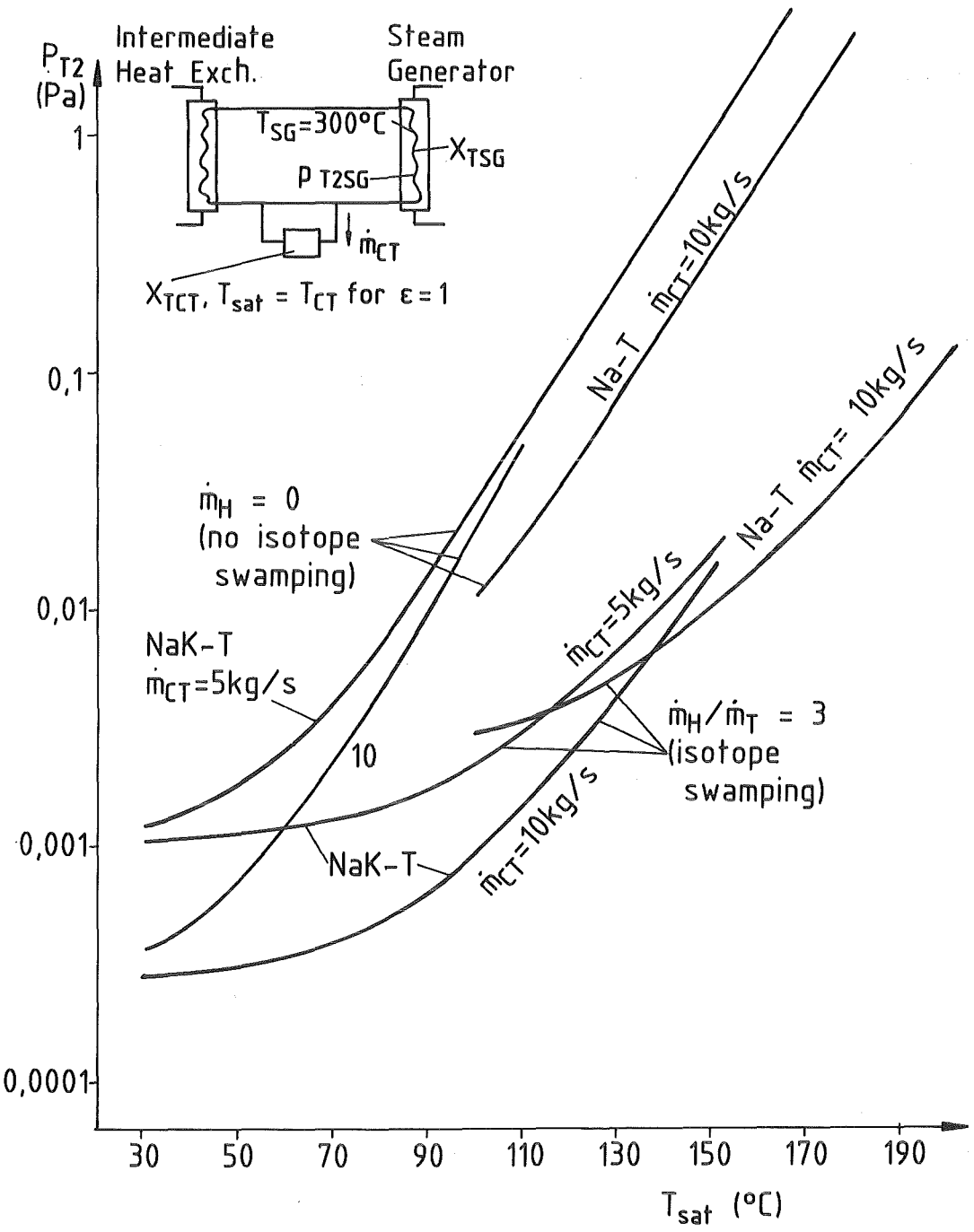

Fig. 20 Effect of Isotope Swamping

fuel clean-up cycle. The enlargement of this unit and the required separation factors represent no technical problem (Bartlit /35/).

Another isotopic effect exists due to the exchange of tritium with hydrogen in solid NaH. The driving force is proportional to the difference between the tritium specific activities in solution and the solid deposit. McPheeters and Raue /34/ developed a model to describe this exchange mechanism and performed experiments. Fig. 21 (from /34/) shows that the isotopic exchange is much less effective than the coprecipitation. However, this effect at least improves the tritium separation if protium exists in larger concentrations than tritium, which will be the normal case.

For the tritium decomposition again additional protium is of advantage in respect to improved decomposition kinetics. Isotope swamping therefore decreases the residual tritium inventory at the end of the decomposition cycle or shortens the decomposition times for a constant residual tritium concentration. It has to be investigated, if the isotopic exchange is of significant influence during the tritium decomposition process.

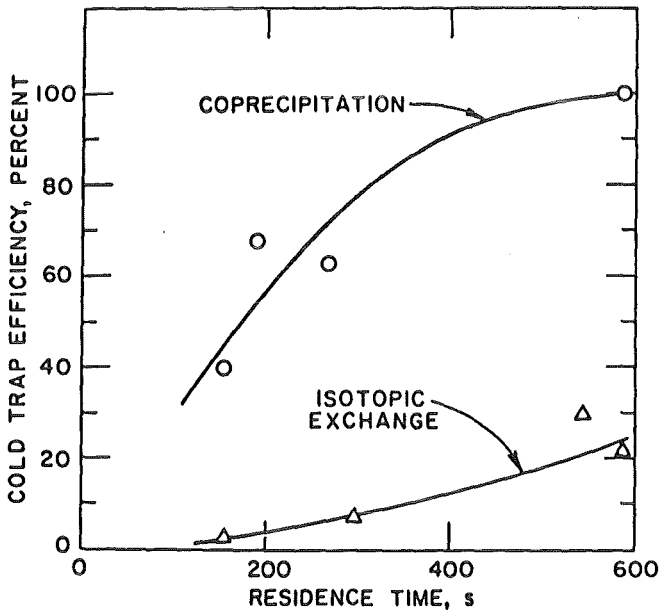

Fig. 21 Cold-Trapping Efficiencies for Co-precipitation and Isotopic Exchange Experiments (from McPheeters and Raue /33/)

3. Experiences with Cold Traps and Improved Designs

Hinze /36/ concludes in his overview on purification methods that "generally, the state of the art is such that the design of purification equipment is chiefly empirical. This is particularly true of cold traps. Operation of cold traps in a number of loops and reactor systems has yielded a considerable amount of information. Even so, no single design has a clearly demonstrated superiority."

This characterization is perhaps too pesimistic for the present state of the art; in the last years the basic understanding has improved and better design tools are available now. However, no "optimized" cold trap has been built and tested yet.

The principle design of cold traps did not change since the first use in the 1950s. Fig. 22 (from Hinze /36/) shows one of the early cold traps: The sodium first is cooled down close to saturation temperature in a regenerative heat exchanger (economizer), heating up the sodium leaving the cold trap. The sodium flows down an annulus which is cooled from the outside by a counter current fluid (gas, liquid metal or organic component, water is avoided due to potential interaction). The lowest temperature is reached at the bottom of the annulus; the sodium flow is then directed upwards and is heated up again and exits at the top. The annulus and/or the inner cylinder usually contains a packing material on which the impurities are supposed to be precipitated or retented by filtration. As packing material wire meshs of different densities have proved to be superior to porous filters or inserts like Raschig rings. However, there is still a controversy on the usefulness, optimal position and density of the wire mesh packing.

Only a few cold traps were analysed in respect to deposition distribution. Often these cold traps were smaller and simpler in design thats those actually used in large sodium loops. In the following, comparisons performed by McPheeters and Raue /28/ between their MASCOT code and experiments are discussed. The references for the different cold traps are also given in /28/.

Fig. 23 shows the design and the comparison for the Billuris cold trap. This cold trap was a simple once-through design with no heat regeneration where the sodium entered the top and flowed downward through the packing and the

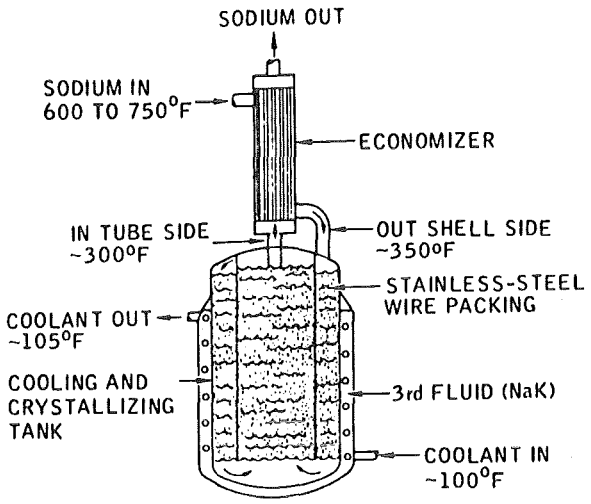

Fig. 22 Knolls Atomic Power Laboratory Cold Trap (from Hinze /36/)

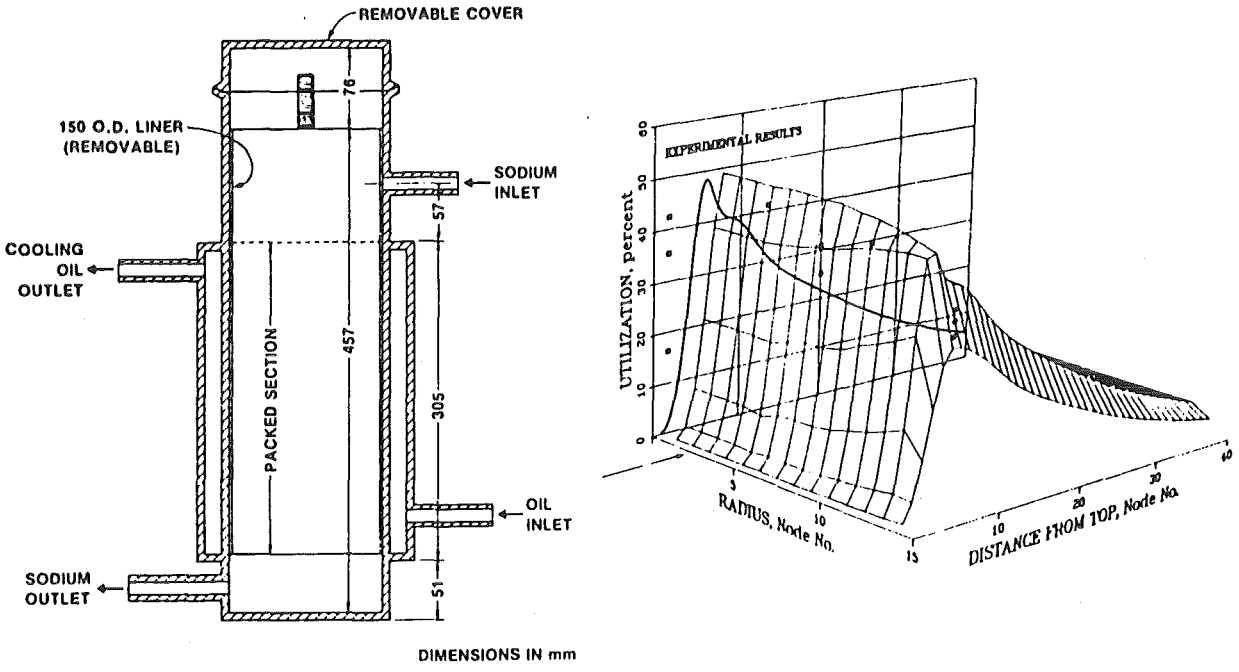

Fig. 23 Design of the Billuris Cold Trap; Experimental Results and MASCOT Calculations (from McPheeters and Raue /28/)

coolant (oil) flowed upward. The comparison is shown on the right hand side of the figure: The orientation is such that the two-dimensional matrix is on the base plane with the centerline of the cold trap along the back, left edge. The volume percent of the loading (here: Na_2O) in each node is plotted vertically at the intersections of the matrix lines. The arrow indicates the sodium flow direction. The experimental results are plotted on the back plane of the figure, along with the radial average of the calculated vol % utilizations. While the average curve does not pass directly through the experimental points, it is clear that the general pattern of impurity deposition is in good agreement between the experimental and calculated cases.

Fig. 24 shows the comparison for the air-cooled MSA cold trap. The MSA cold trap had sodium flow downward through an unpacked, narrow annulus, flow reversal at the bottom, and upward flow through a relatively large packed section in the center.

The agreement between the experimental and calculated distributions is good. The Na_2O deposit is concentrated at the bottom of the mesh section. The reason for this seems to be that the sodium is cooled below the saturation temperature in the annulus, where little solid surface area is available for precipitation. The solution becomes supersaturated, and, when it enters the mesh, a large surface area is suddenly available and profuse precipitation occurs quickly.

An interesting feature are the large peaks of predicted mass deposition in the annulus region. The annulus is not packed in this case: thus, the only surface available for precipitation is the wall surface. In the actual cold trap, the Na_2O that deposited on the walls of the annulus probably accumulated to a critical size, then broke off the wall and fell to the bottom of the cold trap. Unsupported Na_2O crystals probably would not have sufficient strength to withstand the hydraulic forces of the sodium flow. This buildup and breakaway phenomenon cannot be modeled with MASCOT.

The comparison with the Fermi cold trap is shown in Fig. 25. Sodium again flowed downward through a very narrow annulus that contained no packing material. A counterflow of NaK in the outer jacked cooled the incoming sodium. The sodium flow direction reversed at the bottom of the trap and continued upward through a very large center region packed with wire mesh.

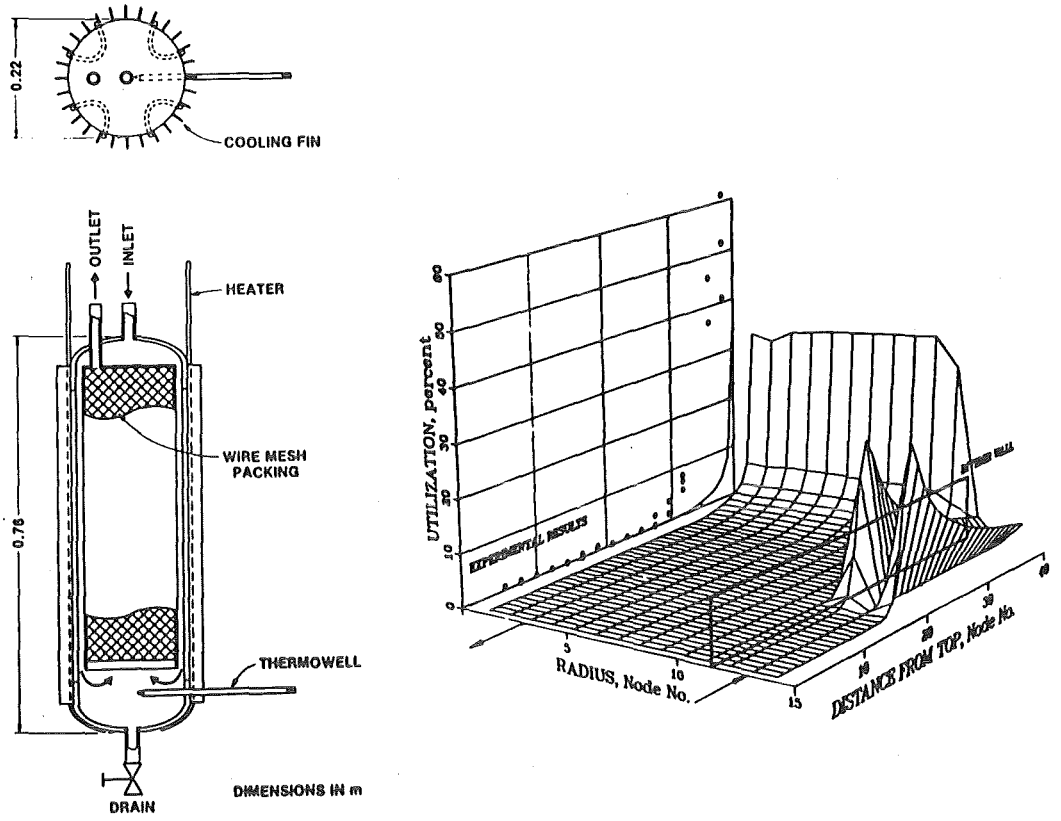

Fig. 24 Design of the MSA Cold Trap; Experimental Results and MASCOT Calculations (from McPheeters and Raue /28/)

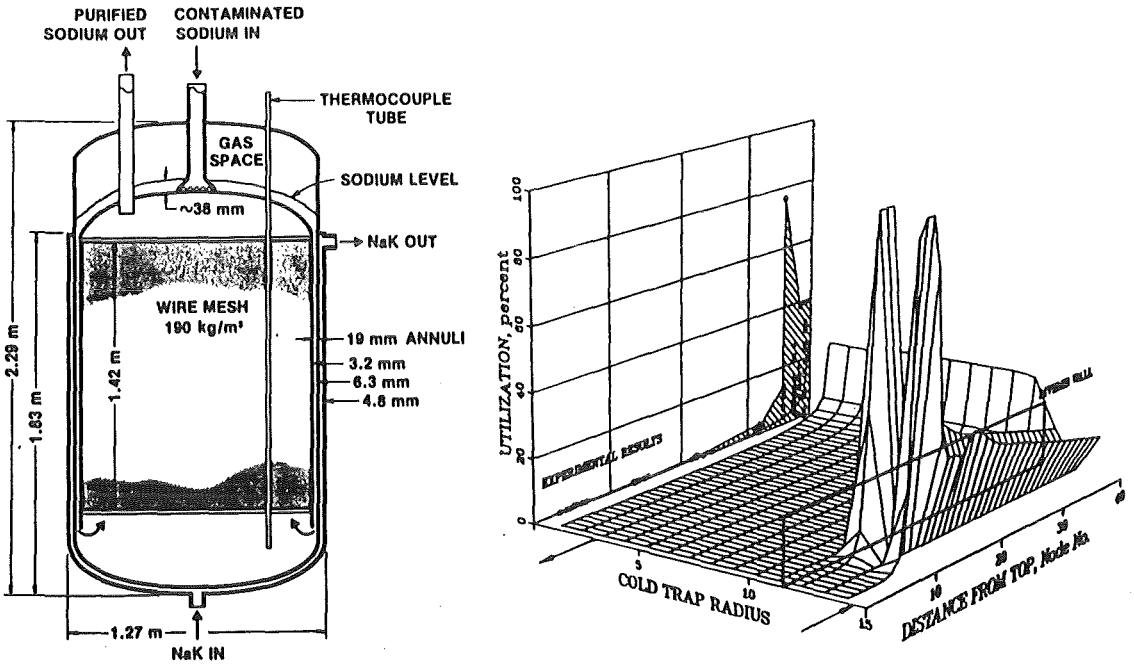

Fig. 25 Design of the Fermi Cold Trap; Experimental Results and MASCOT Calculations (from McPheeters and Raue /28/)

After the cold trap had become plugged, it was removed, and samples were taken for analysis of impurity distributions. Unfortunately, the annulus section was not sampled.

MASCOT calculated the plugging of the cold trap due to the built up of deposits in the annulus. In the experiments plugging occurred in the lower mesh section. The code also predicts a sharp increase of deposit rate in this area.

Special experiments from McPheeters and Raue /28/ to test their code are shown in the next two figures. The design of the ETC 1 cold trap is very similar to the MSA cold trap (Fig. 26). Very little Na_2O is deposited in the annulus, in contrast to the large amounts calculated for the MSA and Fermi cold traps. This effect is probably due to the very low oxygen concentration in the inlet sodium in the ECT1 case, which provided a much smaller source of impurities for deposition on the ECT1 walls. Visual observation confirmed that little deposition occurred in that location. Agreement between the MASCOT calculation and the experimental measurements is excellent.

The second cold trap was originally designed as a scale model of the cold trap for the Clinch River Breeder Reactor (CRBR). The hydrogen deposition was essentially all concentrated in the upper part of the annulus region, and the agreement between the model calculation and the experimental results is good (Fig. 27). The position of the NaH deposit is a direct result of the operating conditions, i.e., the hydrogen concentration at the inlet was high (1.2 ppm) and constant during the entire experiment.

In the past cold traps were investigated with no packing material at all (meshless or packless cold traps). Often concentric baffles were inserted to increase the surface. The results were contradictory: the Hallam Nuclear Power meshless cold trap shown schematically in Fig. 28, presented more operational problems than the packed trap (Hinze /36/), whereas Goodman /37/ points out that meshless traps can be operated under conditions insuitable for mesh-packed traps - high flow rates combined with large concentration gradients. The explanation given for this is "the larger the concentration gradient, the more localized the nucleation of crystals. In meshless traps this causes plugging of the mesh and loss of flow. Without mesh the impurities precipitate to the bottom of the trap. This removes then from the flow

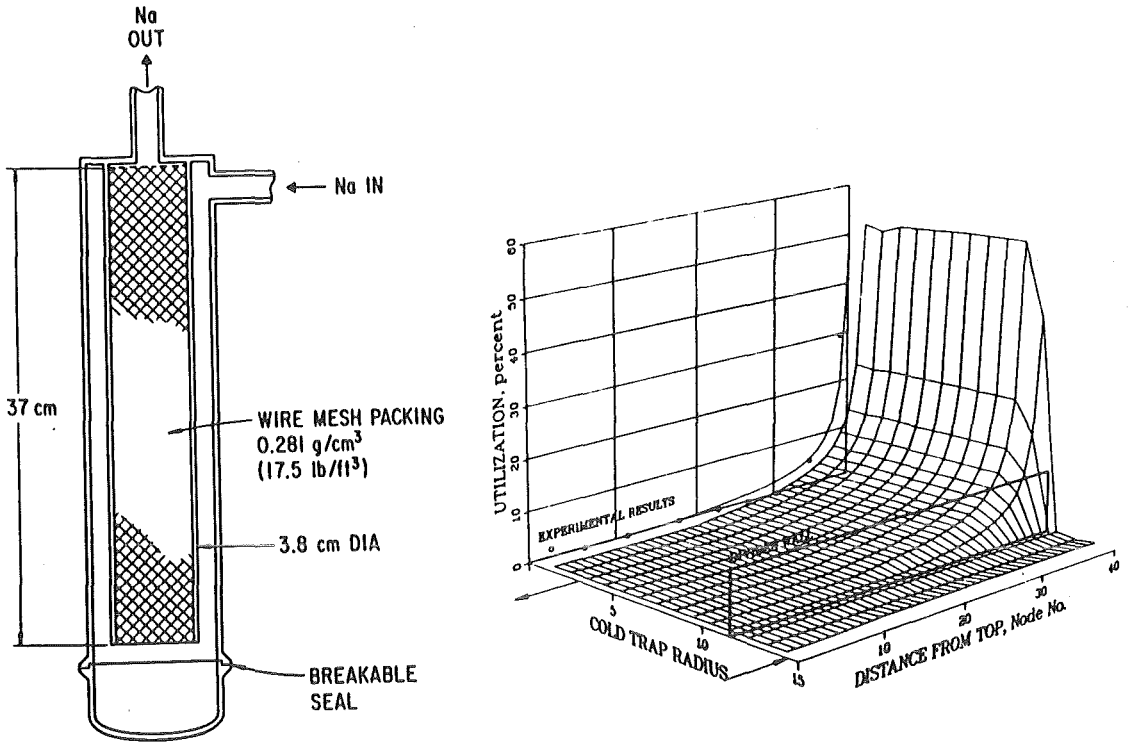

Fig. 26 Design of the ETC1 Cold Trap;
Experimental Results and MASCOT Calculations
(from McPheeters and Raue /28/)

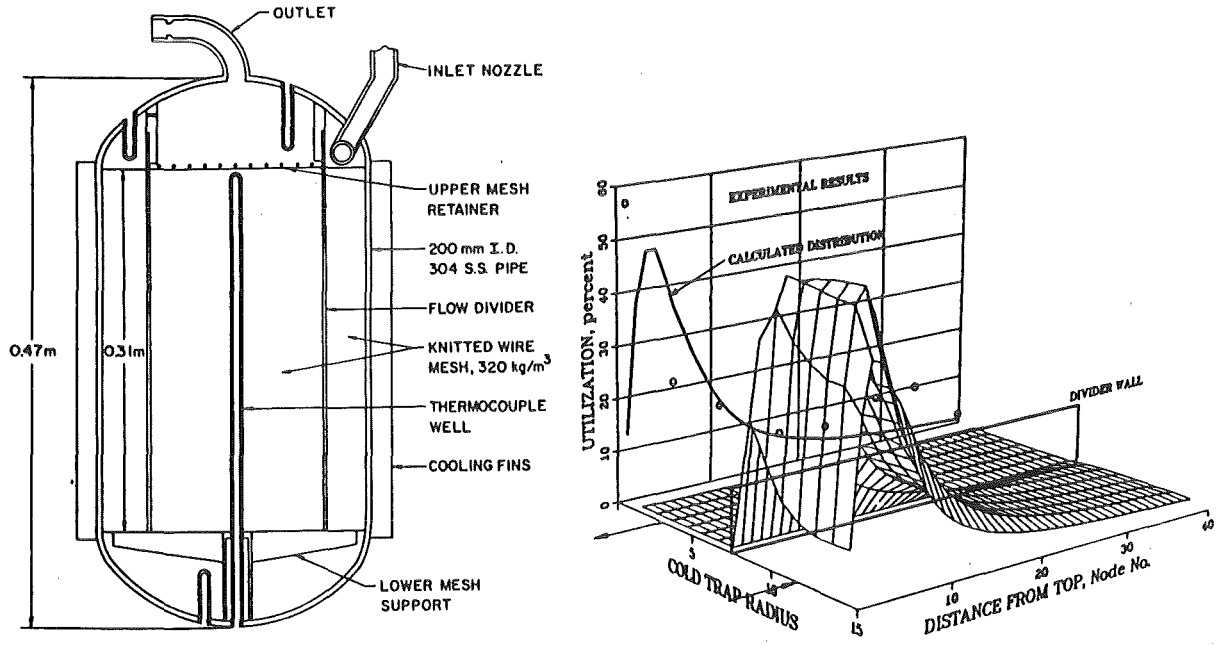

Fig. 27 Design of CRBR Cold Trap;
Experimental Results and MASCOT Calculations
(from McPheeters and Raue /28/)

stream and precludes plugging".

Another design concept was to devide the cold trap in a cooling, settling and filtration zone. Fig. 29 (from Hinze /36/) shows the schematical set-up and some results. The precipated masses were about equal in the three zones. Again it was argued that packing is not required as sites for cristallization since 65 % of the impurities trapped remained in the cooling and settling zones which did not contain packing.

A cold trap with a large packed annulus and a relatively small unpacked center region is shown in Fig. 30 (from Hinze /36/). To increase the trap capacity this design includes a bypass line containing a flow-control valve, around the economizer section of the trap. The bypass was incorporated to eliminate complete dependency on reduced cold-trap inlet flow when intratrap temperature regulation is required. This bypass could give the operators means for preventing formation of oxide crystals upstream of the mesh section, for distributing oxide deposition in the trap when sodium feed to the trap is saturated with oxygen, and for redistributing oxide in the mesh section when the feed is no longer saturated; however, precise placement or redistribution of oxide deposits is difficult to achieve. At a minimum, additional temperature sensors in the mesh section would be required.

The previous sections have shown that there is a considerable discrepancy on the optimal design of cold traps. The propper design is strongly affected by the broad range of impurity inlet concentration; starting with a value of about 100 ppm at beginning of operation and going down to values of about 1 ppm. If the inlet concentrations vary much less, for instance due to an additional cold trap for the start-up phase, the conclusions drawn by McPheeters and Raue /28/ propably represent best the present state of the art:

1. Narrow flow passages should be avoided in regions where the sodium temperature is being reduced in the impurity-saturation range. Impurities will deposit in these regions and possibly plug the flow passage.
2. A large volume having an abundance of nucleation sites should be provided in the region of the cold trap where precipitation of impurities first begins. This region will accumulate most of the impurity burden of the sodium systems.

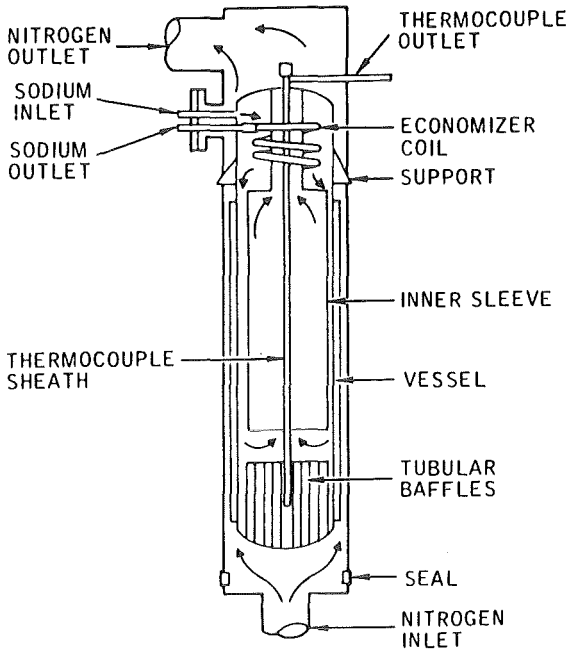

Fig. 28 Hallam Nuclear Power Facility Experimental Cold Trap Without Packing (from Hinze /36/)

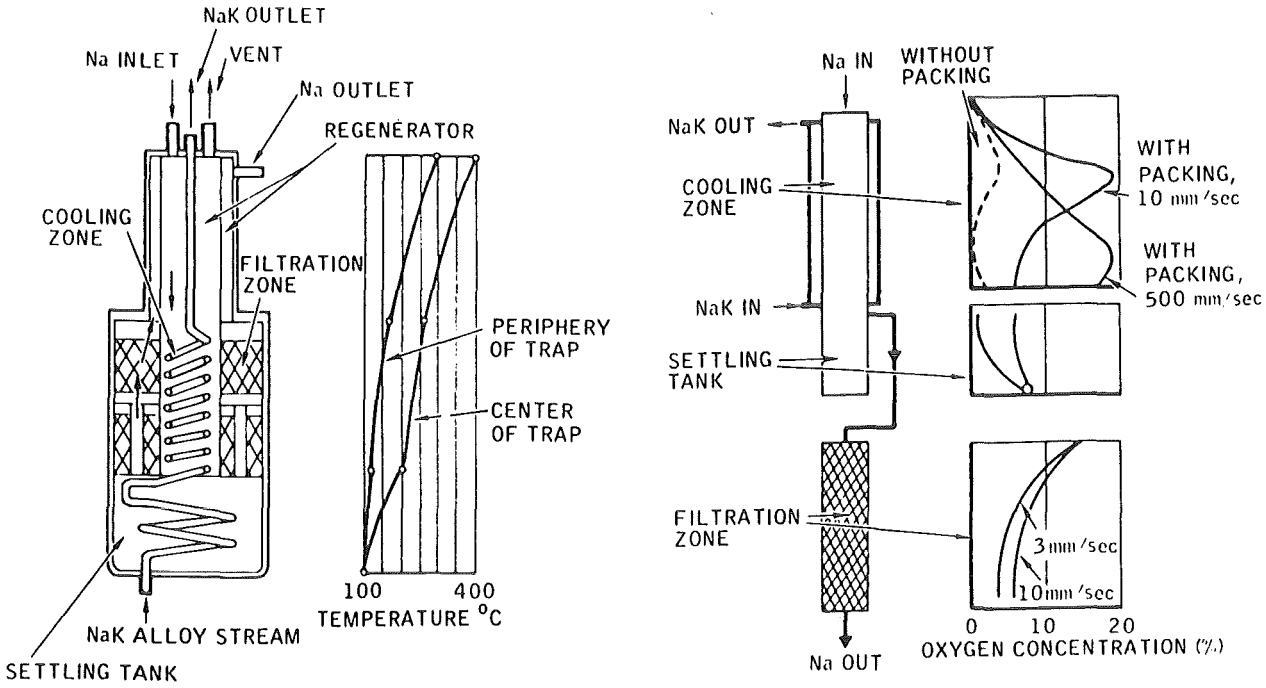

Fig. 29 USSR Cold Trap and Generalized Results (from Hinze /36/)

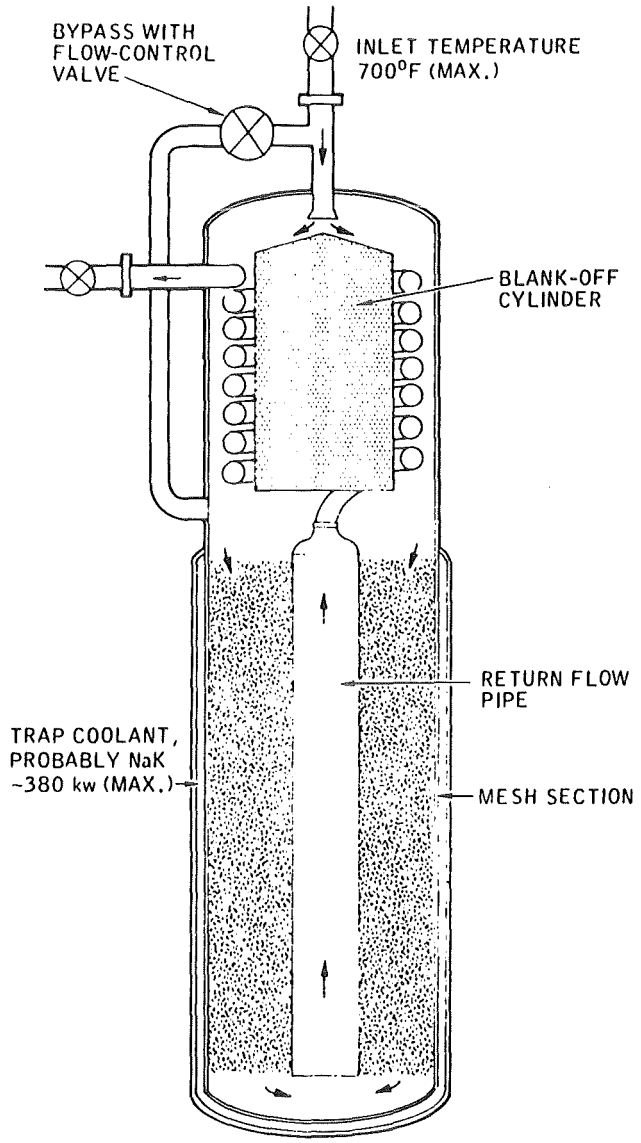

Fig. 30 Proposed Fast Flux Test Facility
Cold Trap (from Hinze /35/)

3. Cold trap designs, having no packing where the sodium is cooled below the impurity saturation temperature and having packing downstream of the cooling region will generally have low capacity. This low capacity is due to the sodium becoming supersaturated in the packless region followed by rapid precipitation of impurities when the packing is encountered. The packing provides many sites for nucleation and growth of impurity crystals.
4. The packing in the center region of a cold trap collects very little impurity deposits when packing is present in the annulus. When the annulus is unpacked, the center region tends to plug quickly. Therefore, the preferred design would have a large, packed annulus and a relatively small, unpacked center region.

4. Considerations for Regenerative Cold Traps for Tritium Recovery

The previous sections presented the state of the art for cold traps to precipitate impurities. Very limited work exists on recovering the hydrogen from the cold trap. The work discussed in Chapter 2.4 was based on the thermal decomposition of the hydrides below 412 °C.

A concept to unload Na cold trap by converting the solid deposits to drainable liquids by the reactions

$$Na_2O_{(s)} + NaH_{(s)} = NaOH_{(l)} + 2\ Na_{(l)} \qquad (19)$$

was proposed by McKee /38/. This reaction proceeds to the right above 412 °C according to Myles and Cafasso /17/. This concept has no advantages for the separation of tritium from Na and is not regarded further.

The following conclusions were drawn from the decomposition experiments:
Not draining the cold trap is disadvantageous because
- bubble nucleation is deteriorated due to the geodetical pressure term in Eq. (14).
- most of the liquid sodium is evaporated during regeneration and has to be trapped in sodium vapor traps.

The argon purge at atmospheric pressure also deteriorates bubble nucleation, compare Eq. (14).

Gas bubbling through the undrained cold trap was not investigated yet. The provison of bubbles and the enhanced mixing may compensate some of the adverse effects and has to be investigated.

The most promising technique for a fusion blanket cold trap is propably to drain the cold trap and decompose the tritide below 412 °C by vacuum pumping. The recovered tritium could be stored with a solid getter or fed into the fuel clean-up cycle to separate residual gaseous impurities.

For a given reactor power, the cold trap mass flow rates are comparable for a fast breeder and a fusion reactor (≈10 kg/s, for the SNR 300 or NET compare Section 5). The substantial difference for the latter application is the

required short regeneration time (some days instead of one year) to feed back the tritium into the fuel cycle and to keep the tritium inventory small for safety reasons. The short regeneration cycle results in a small cold trap loading. Therefore, the cold trap dimensions could be considerably smaller. In respect to tritium inventory there is no strong need to minimize the cold trap volume. A retention time of 5 minutes typical for fast reactor cold traps, would result in a tritium inventory of less than 4 g for the example discussed in Section 5 which seems to be quite acceptable. Due to the fact that oxygen and other impurities accumulate in the cold trap, the dimensions should be large enough that no plugging occurs during several years of operation. This seems not to be unreasonable because prior to tritium operation, the loop should be appropriately cleaned (additional cold and or hot trap).

A proper design for a regenerative cold trap differs considerably from that for a nonregenerative cold trap:

- if the cold trap is drained the bottom zone should not be the coldest zone to avoid plugging of the draining lines
- the growth of cristals with large surfaces (dendrites) is desired because hydrogen release is strongly dependent on the specific surface
- the design should be simple to allow remote handling (exchange of packing etc.) due to the potential built-up of radionuclides.

These points are taken into account in the conceptional design shown in Fig. 31:

- The cold trap is "reversed" compared to previous applications. The drainage lines are in the hot zone. To prevent plugging of the drainage lines due to broken cristals a mesh packing serving as a filter is located near the bottom. This reversed cold trap is more sensitive to the development of a secondary flow due to free convection than the conventional cold trap. The design has to prevent the development of a vortex with a downward velocity near the cold outer cylinder.
- Precipitation should occur in the large packing annulus where the velocities are low to enhance dentrite growth.
- Precipitation at the top cap and in the unpacked center region should be avoided to prevent plugging of the center line drainage line. Therefore the upper part of the outer cylinder and the top cap is slightly heated.
- As coolant and heating fluid the same fluid as in the cold trap should be used. During the decomposition phase the heating fluid should be a bypass

stream from the main loop. Thus a tritium built-up in the heating fluid due to permeation is prevented.

- The economizer is separated from the precipitation zone. This results in a smaller volume to be drained and thermally cycled.

Fig. 32 shows schematically the tritium processing unit. One cold trap is loaded while the other is deloaded, a third cold trap (not shown here) is in standby.

To recover the tritium the heated cold trap is connected with the vacuum pump. The evaporated Na or NaK is condensed in two vapor traps, the hydrogen isotopes are gettered with a suitable getter material or are fed directly into the fuel clean-up system to remove residual impurities.

In the next chapter, some calculations are made to apply this tritium separation method for a self-cooled blanket for NET.

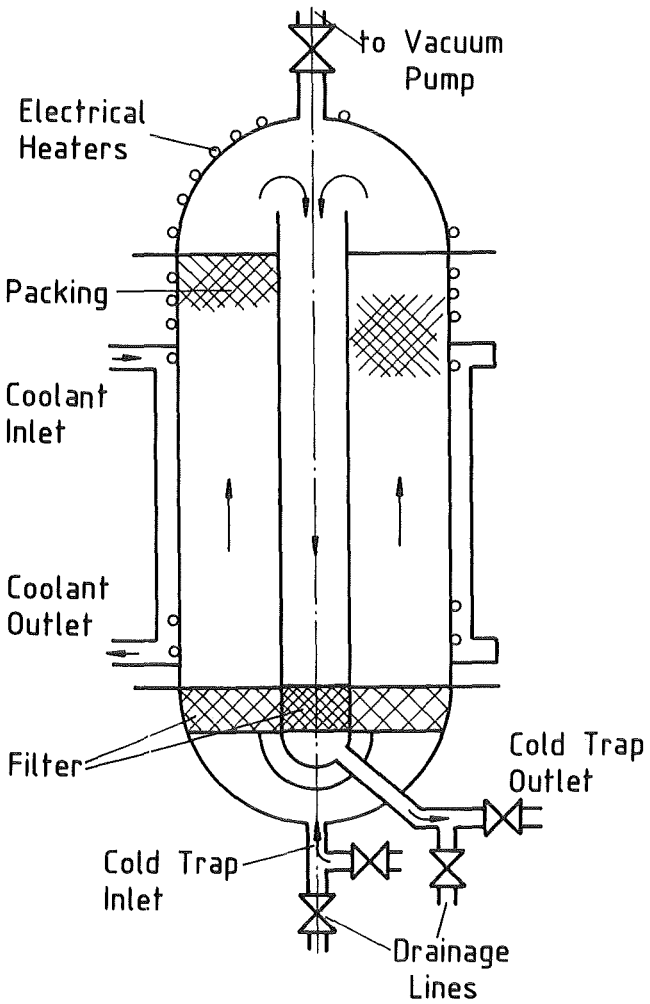

Fig. 31 Conceptional Design of Cold Trap for Tritium Precipitation and Recovery

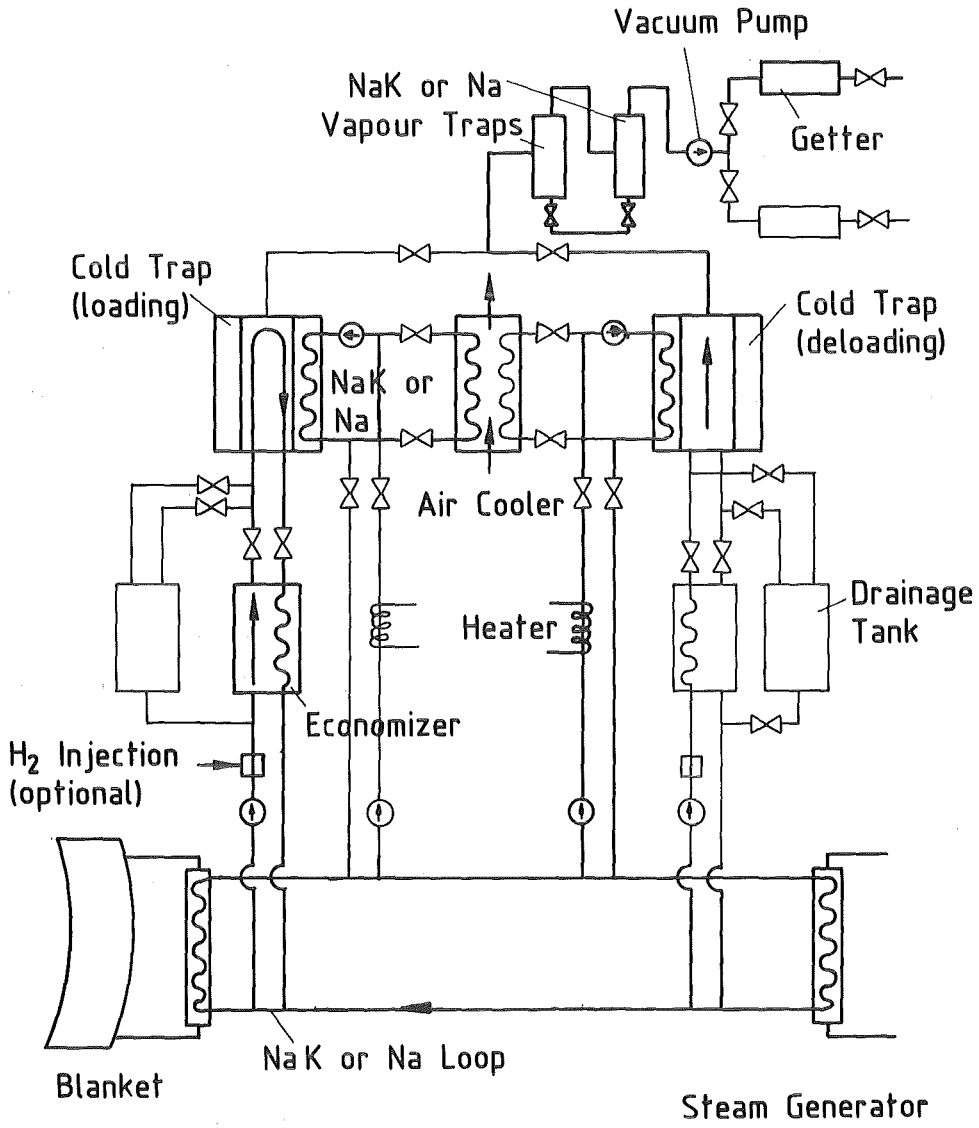

Fig. 32 Tritium Separation and Recovery in the Intermediate Loop

5. Tritium Separation System for the NET Blanket

5.1 Tritium Separation in an Intermediate Sodium Loop

The following calculations are made for the case of a selfcooled LiPb blanket and a Na secondary circuit. NaK would result in more favourable values but the present technology is more developed for Na. The tritium is only separated in the secondary loop.

The design parameters for the secondary loop are nearly identical to those of the fast breeder SNR-300, (see e.g. Leeuwen et al. /39/). The heat flux density in the intermediate heat exchanger of that reactor is 0.21 MW/m^2. If the same heat exchange design is used for NET, the necessary surface is A = 3000 m^2. The same surface is assumed for the steam generator.

The total liquid metal flow rate into the cold traps of the SNR-300 is for comparison 4 x 2,36 kg/s. In accordance to that design a total flow rate of 10 kg/s has been selected for the NET cold traps which is 0.2 % of the flow rate in the secondary loop.

Fig. 33 shows the layout and the design parameters for the heat and tritium extraction system. With the tritium production rate of m_T = 50 g/day = 0.58 10^{-6} kg/s the permeation flux through the heat exchanger tubes is

$$\dot{m}_T/A = 1.9\ 10^{-10}\ kg/s\ m^2$$

The tritium concentration in the LiPb depends on the tritium concentration in the secondary liquid metal and additionally on the following steps:

a) Transport through the LiPb boundary layer
b) Permeation through the wall
c) Transport through the Na boundary layer

A rough estimate using mass transfer coefficients of β_{LiPb} = 0.05 cm/s and β_{Na} = 0.5 cm/s shows clearly that the resistances involved in step a) and c) are small compared to the permeation resistance of step b) and are therefore neglected.

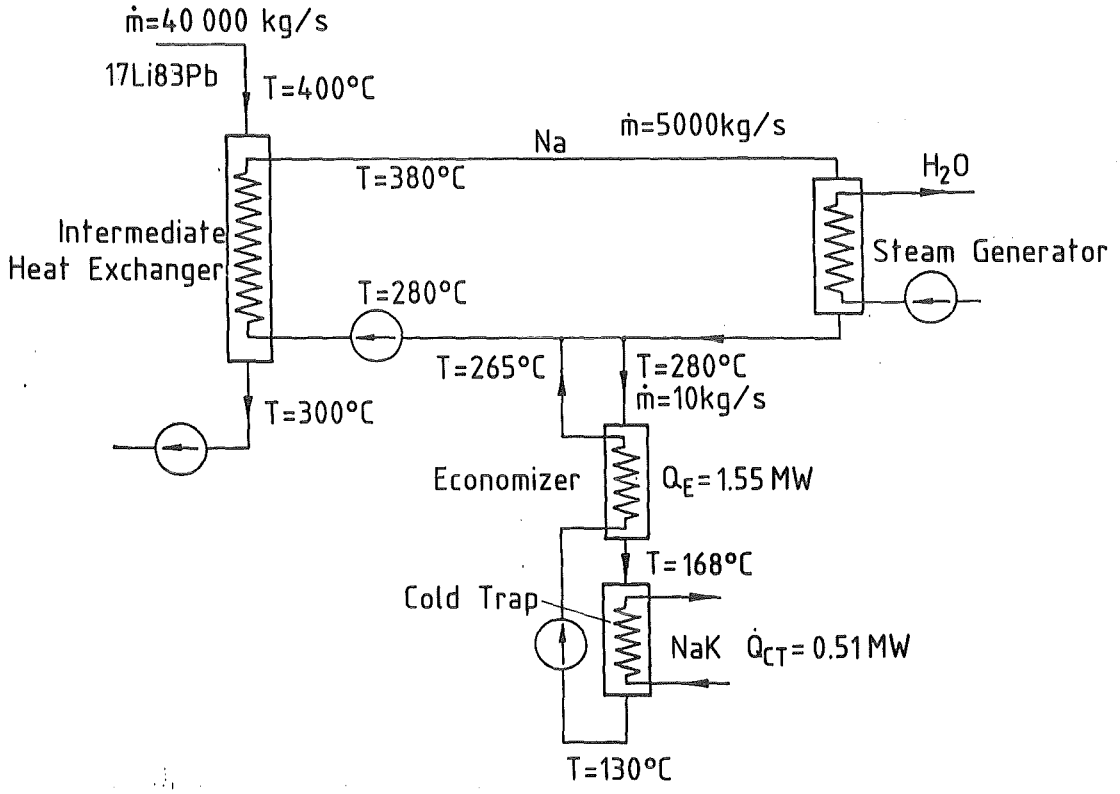

Fig. 33 Temperatures and Mass Flow Rate in the Intermediate Sodium Loop for NET

5.1.1 Tritium Concentration in Sodium

To reduce the tritium concentration at the outlet of the cold trap, protium is added at the entrance to the cold trap bypass with a mass flow ratio of

$$\dot{m}_H/\dot{m}_T = 3$$

This isotope swamping mass flow ratio results in a ten times higher atomic hydrogen concentration. The value of 3 is considerably smaller than the value of 10 assumed by Sze /5/ in his tritium separation concept.

To determine the tritium cold trap outlet concentration, Eq (2) for NaH is converted to atomic concentrations

$$\ln x_{CT}\ (\text{appm}) = 18 - 6961/T(K) \qquad (20)$$

For a saturation temperature of 150 °C this results in a total hydrogen concentration of

$$x_{CT} = 4.68\ \text{appm}.$$

Only one tenth of the atoms are tritium atoms, therefore

$$x_{T\ CT} = 0.468\ \text{appm} = 0.061\ \text{wppm}$$

The cold trap efficiency is smaller than one. To obtain the concentration given above at the outlet of the cold trap, the cold trap temperature T_{CT} has to be lower. For T_{CT} = 130 °C the hydrogen concentration is

$$x_{sat\ CT} = 2.07\ \text{appm},$$

respectively,

$$x_{Tsat\ CT} = 0.207\ \text{appm} = 0.027\ \text{wppm}$$

The tritium concentration at the inlet of the cold trap x_{in}(wppm) is calculated with Eq.(4)

$$x_{in} = 0.119 \text{ wppm}$$

With the cold trap efficiency defined by

$$\mathcal{E} = (x_{in} - x_{T\ CT})/(x_{in} - x_{Tsat\ CT}) \qquad (21)$$

a value of $\mathcal{E} = 0.63$ is obtained which corresponds fairly well to a 5 minutes residence time, compare Fig. 12.

The tritium pressures in the sodium system are determined from Eq (1), calculating $K_T = 3 \cdot K = 1.19$ from Eq (2) and are shown in Fig. 34.

5.1.2 Tritium Permeation through the Intermediate Heat Exchanger Tubes

A relationship provided by Renner and Raue /40/ is used because the conditions in their experiments were very similar to the case of an intermediate heat exchanger for NET, i.e.

- ferritic steel as heat exchanger material
- liquid metal at the upstream surface of the wall
- clean (unoxidized) surface at the downstream side
- tritium as diffusing isotope
- wall temperature 673 K

The tritium permeability Perm is given by:

$$\text{Perm}[mm^3(STP)T_2\ mm/sm^2Pa^{0.5}] = 769 \cdot \exp(-39140(J/mol)/R \cdot T \qquad (22)$$

The tritium permeability at 673 K as calculated by Eq (22) is compared to other references in Table IV.

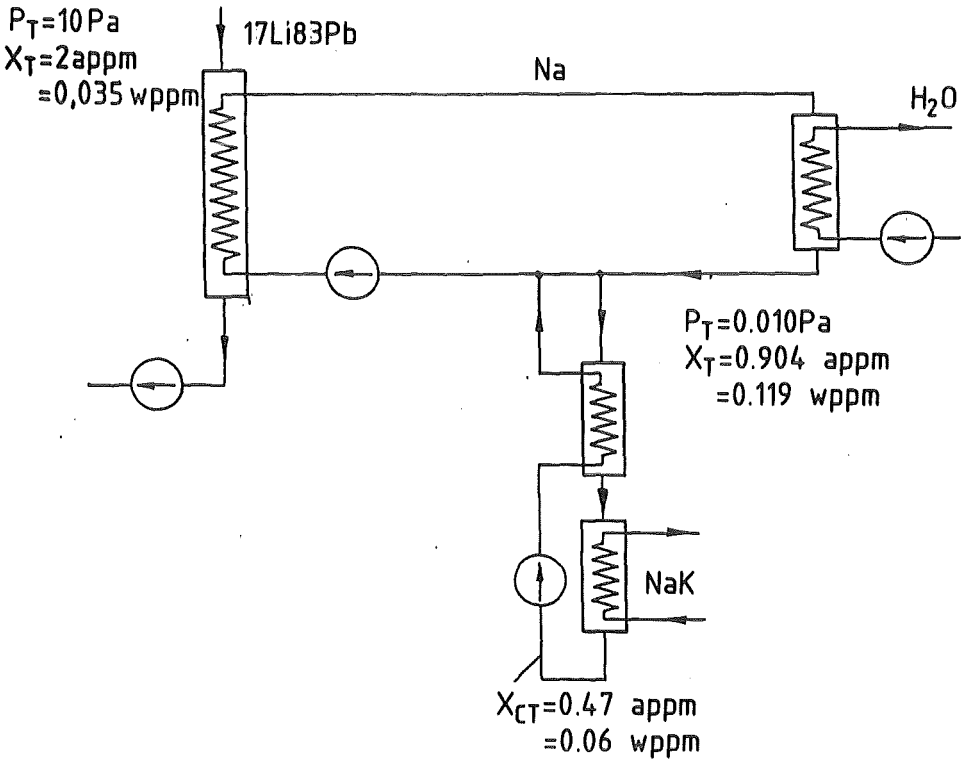

Fig. 34 Tritium Concentrations and Partial Pressures in the Intermediate Sodium Loop for NET

Reference	T-Permeability of ferritic steel at 673 K Ci/(d m $Pa^{0.5}$)
Renner and Raue /40/	0.163
Maroni and Van Deventer /41/	0.365
Starfire /42/	0.3
DEMO /2/	0.2
BCSS /4/	0.2

Table IV: T Permeability of Ferritic Steel

For a mean temperature of 350 °C and a wall thickness of 1.5 mm the following value is obtained

$$\text{Perm} = 0.402 \; \frac{mm^3 \; (STP) \; mm}{s \; m^2 \; Pa^{0.5}}$$

$$= 0.93 \cdot 10^{-2} g \; mm/(d \; m^2 Pa^{0.5})$$

the tritium partial pressure in the LiPb is calculated by means of

$$\dot{m}_T = \frac{\text{Perm } A}{s} \; (P_{T2,LiPb}^{0.5} - P_{T2,Na}^{0.5}) \qquad (23)$$

For $p_{T2,Na}$ = 0,01 Pa a value of $p_{T2,\ LiPb}$ = 7,84 Pa is obtained. For a Sieverts constant of $K_{T,LiPb} = 6.3 \cdot 10^{-7}$ (mol T/mol LiPb)/$Pa^{0.5}$ from Wu /12/, a tritium concentration of $x_{T,\ LiPb}$ = 1,7 appm = 0,029 wppm is calculated.

For 300 m^3 LiPb corresponding to ≈ $3000 \cdot 10^6$ kg LiPb a tritium inventory of

$I_{T,\ LiPb} \approx 87$ g is obtained.

For 300 m^3Na corresponding to ≈$300 \cdot 10^3$ kg Na the Tritium inventory is

$$I_{T,Na} = 300 \cdot 10^6 g \cdot 0,119 \cdot 10^{-6} \approx 36 \; g$$

A rough estimate shows that the tritium inventar in the steel is less than 1 g.

5.1.3 Double Walled Heat Exchanger between Lithium-Lead and Water

Double walled heat exchanger were proposed in the BCSS /4/ and MARS /43/ in connection with lithium-lead breeder blankets in order to lower tritium permeation to the cooling water. In all of these concepts, a helium purge stream which contains a small amount of oxygen, flows through the double wall space. The intention is to

a) oxidize tritium to T_2O in order to lower permeation

b) oxidize the wall surfaces, providing permeation reducing layers.

Contrary to this concept it is proposed here to have a liquid metal or a molten salt flowing through the double wall space.

Fluids with a high tritium solubility are favourable in order to maintain a low tritium partial pressure in the gap. An additional requirement is a suitable method to extract tritium from the secondary liquid metal. Sodium is one possible material as it has been shown in Section 5.1. A small fraction (0.2 % ≙ 10 kg/s) of the sodium flow in the secondary loop is processed in the cold trap for tritium extraction.

The same flow rate of 10 kg/s is used as purge flow in the gap and through the cold trap as it can be seen in Fig. 35. Fig. 36 shows the schematic design of a double walled heat exchanger which is a modification of the single walled steam generator for the SNR-300. The gap size between the two tubes is 1 mm. 2000 tubes are necessary for a heat exchanger area of 3000 m^2 and a tube length of 20 m. The resulting sodium velocity in the gap is 5 cm/s and the pressure drop roughly 20 Pa. In a more detailed design the problems of leak detection and repairability have to be considered.

Tritium concentration and -inventar in the LiPb are identical to the case of a secondary sodium loop discussed in Chapter 5.1.1. The tritium inventar in sodium however is reduced from 36 g to 1 g due to the much smaller sodium mass.

5.1.4 Tritium Permeation Losses to the Cooling Water

If the tube walls between sodium and water are made of austenitic steel, the permeability can be calculated with the relationship given in the BCSS /4/:

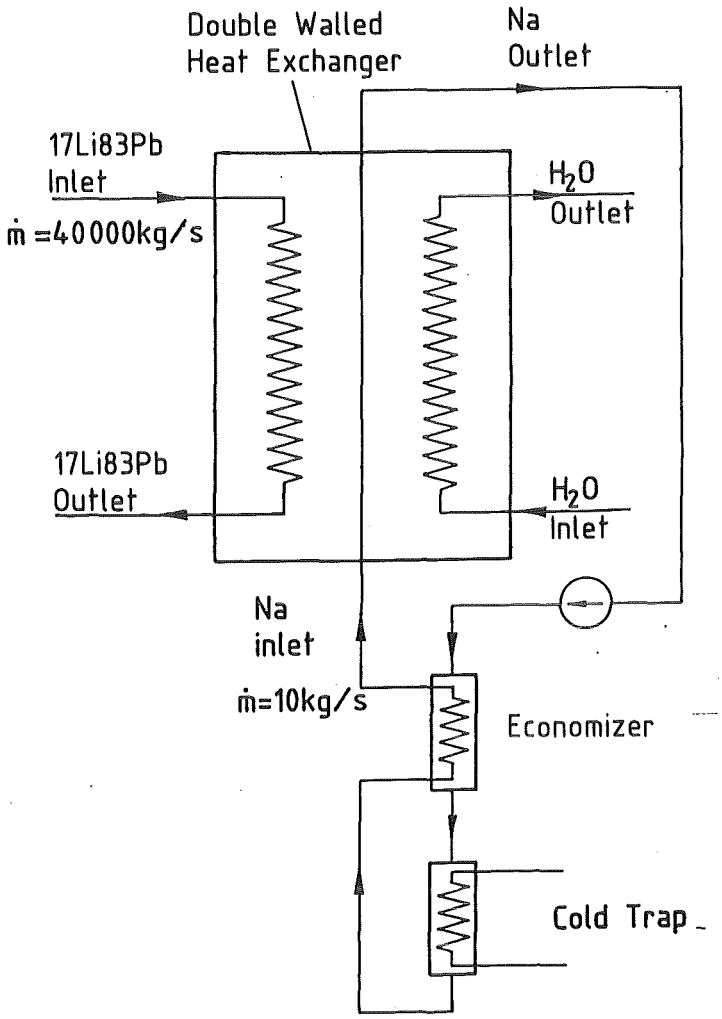

Fig. 35 Flow Sheet for Double Walled Heat Exchanger with Cold Trap

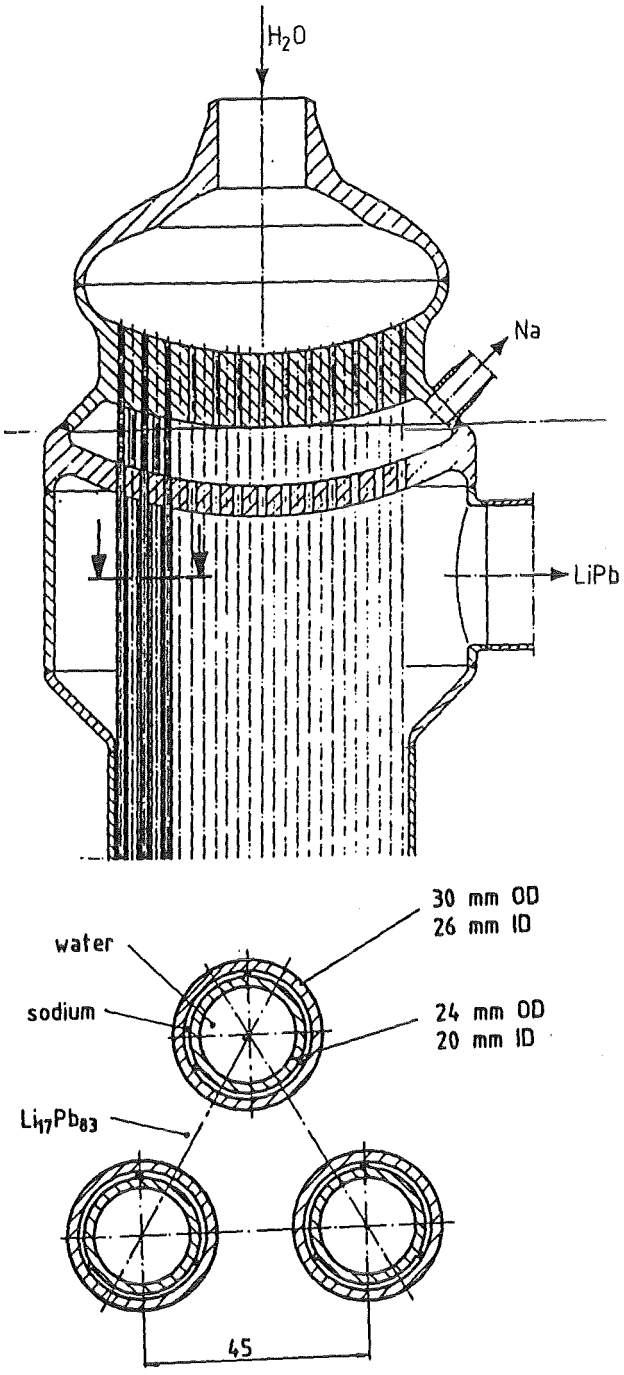

Fig. 36 Schematic Design of Double Walled Heat Exchanger

$$\text{Perm} = \frac{2.33 \cdot 10^{-2}}{\sqrt{T}} \; \frac{\text{cm}^3(\text{STP})}{\text{cm s atm}^{0.5}} \exp(-15700\,(\text{cal/mol})/RT) \qquad (24)$$

A mean temperature of 300 °C results in

$$\text{Perm} = 1.16 \cdot 10^{-12} \text{g}/(\text{ms Pa}^{0.5})$$

The tritium flux to the water for clean unoxidized tubes is

$$\dot{m}_{T,\text{Perm}} \approx \text{Perm} \cdot \frac{A}{s} \cdot \sqrt{p_{T2,\text{Na}}} = 1.16 \cdot 10^{-12} \cdot \frac{3000}{0.002}$$

$$\approx 1.74 \cdot 10^{-7} \text{g/s} = 174 \text{ Ci/d}$$

This permeation loss will be reduced by an oxide layer at the water side by at least a factor of 10, avoiding the need for an isotopic separation plant for processing the cooling water.

5.2 Other Options

5.2.1 Use of NaK instead of Na in the Intermediate Loop

Due to the lower cold trap temperature of NaK the maximum allowable tritium partial pressure of $p_{T2} \approx 10^{-2}$ Pa can be reached without isotope swamping, compare Fig. 10.

A tritium partial pressure $p_{T2} = 0{,}01$ Pa is reached by

- a cold trap mass flow rate of $\dot{m}_{CT} = 10$ kg/s at $T_{sat} \approx 89$ °C. Assuming a cold trap efficiency of $\varepsilon = 0{,}6$, this corresponds to a cold trap temperature of $T_{CT} = 83$ °C.
- a cold trap mass flow rate of $\dot{m}_{CT} = 5$ kg/s at $T_{sat} = 84$ °C. With $\varepsilon = 0{,}6$ a cold trap temperature of $T_{CT} = 73$ °C is necessary.

These cold trap temperatures do not appear to be unreasonably low.

With isotope swamping lower tritium partial pressures can be reached which decreases tritium permeation and reduces the tritium inventory both in the NaK and the LiPb system. This is demonstrated by means of the following example:

For a saturation temperature $T_{sat} = 80$ °C and $\dot{m}_H/\dot{m}_T = 3$ a tritium outlet

concentration of x_{CT} = 0.019 wppm is calculated. For $\varepsilon \approx 0.6$, the cold trap temperature is then T_{CT} = 70 °C. For $\dot{m}_{CT}$ = 10 kg/s, the inlet concentration is x_{in} = 0.077 wppm, corresponding to a partial pressure of $p_{T2} = 4.7\ 10^{-4}$ Pa. This value results in a tritium loss through the unoxidized steam generator tubes of 38 Ci/d, compared to 174 Ci/d for Na. The lower partial pressure in the NaK loop requires a lower tritium partial pressure in the LiPb loop of $p_{T2\ LiPb}$ = 7.35Pa, compared to 7.84 Pa. The tritium inventory in the NaK and LiPb loops reduce to 20 g and 80 g compared to 38 g and 87 g.

5.2.2 Tritium Separation in the Primary and Secondary Loop

In the tritium reprocessing concept of Natesan and Smith /11/ for a fusion power reactor the allowable tritium partial pressure in the secondary loop could only be reached by an additional tritium separation unit in the primary system. The idea is to extract the largest part of the bred tritium in the primary loop and thus to reduce the tritium mass flow rate into the secondary loop. To achieve this, a low tritium permeability of the heat exchanger material is desired.

The concept of using processing systems in both loops for NET conditions appears favourable if

a) the two processing systems together become smaller and with this the total costs compared to one system.
b) the tritium inventory in the total system decreases.

First topic a) is addressed: Generally, the size of processing system decreases with increasing inlet concentration that is with increasing tritium partial pressure. An increase of the tritium partial pressure in the primary loop is obtained by using an intermediate heat exchanger material with a lower tritium permeability. Therefore, an austenitic material is taken instead of a ferritic one which results in about a 10 times smaller permeability.

For two processing systems the tritium concentration in the secondary loop is calculated by

$$x_{in} = x_{CT} + C\dot{m}_T/\dot{m}_{CT} \qquad (24)$$

where C is the factor of permeated tritium mass flow rate into the secondary loop $\dot{m}_{perm}$ to the bred tritium mass flow rate $\dot{m}_T$. The tritium partial pressure is then determined with Eq. (1).

Fig. 37 shows that for a cold trap mass flow rate of m_{CT} = 10 kg/s and a cold trap efficiency of $\varepsilon = 1$ ($T_{sat} = T_{CT}$) the influence of the reduced tritium mass flow rate characterized by the factor C. The tritium partial pressure is decreasing with decreasing C; however, the effect is not considerable if one takes into account that the tritium permeation into the steam generator is proportional to $P_{T2\ SG}^{0.5}$.

In order to determine how this reduction of the tritium mass flow rate into the secondary loop can be achieved, the primary loop is regarded. The tritium mass flow rate separated in the processing unit (index pu) is

$$\dot{m}_{T\ pu} = \dot{m}_T - \dot{m}_{perm} \tag{25}$$

$\dot{m}_{perm}$ is given by:

$$\dot{m}_{perm} = \rho_w \cdot (A/s) \cdot D(x_1 - x_2) \tag{26}$$

where D is the tritium diffusivity in the wall material, ρ_w the density of the wall, and the index 1 and 2 denote the primary and secondary loop.

With

$$\dot{m}_{T\ pu} = (x_{in\ 1} - x_{out\ 1})\dot{m}_{pu}, \tag{27}$$

where x_{out1} is the tritium concentration at the outlet of the processing unit 1 and with $x_2 \ll x_1$

one obtains for $x_1 = x_{in\ 1}$

$$x_{in\ 1} = (1+\rho_w DA/(\dot{m}_{pu}s))^{-1}(x_{out\ 1}+\dot{m}_T/\dot{m}_{pu}) \tag{28}$$

and

$$C = \dot{m}_{perm}/\dot{m}_T = (1+x_{out\ 1}\ \dot{m}_{pu}/\dot{m}_T)(1+\dot{m}_{pu}/C') \tag{29a}$$

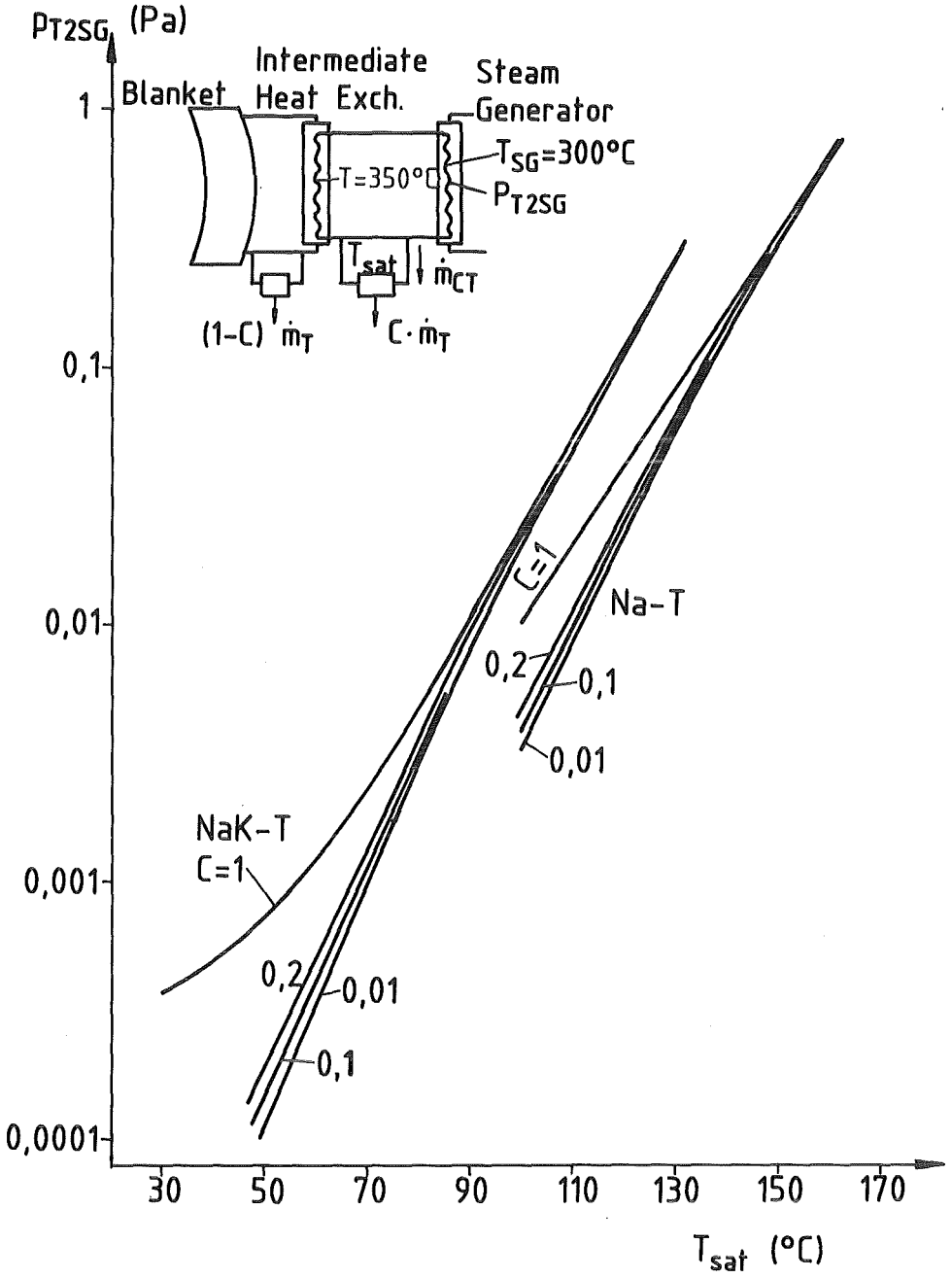

Fig. 37 Influence of Reduction of Tritium Mass Flow Rate in Secondary Loop ($\dot{m}_{CT}$ = 10 kg/s)

where

$$C' = \varsigma_w DA/s \qquad (29b)$$

with A = 3000 m^2, s = 0.0015 m, ς_w = 8000 kg/m^3, and D for 316 SS according to Tanabe et al. /44/:

$$D(m^2/s) = 6.23 \cdot 10^{-7} \exp(-47.8(kJ/mol)/RT) \qquad (30)$$

one obtains with R = 8.314×10^{-3} kJ/mol K and T = 350 °C : C' = 0.98 kg/s.

Fig. 38 shows the reduction of the tritium mass flow rate into the secondary loop as a function of the mass flow rate to the tritium processing unit in the primary loop for different values of the corresponding tritium outlet concentration. The same figure contains also the corresponding tritium inventory calculated with the help of Eq. (28) and assuming again a LiPb mass of 3×10^6 kg.

Presently it is not known, which values for $x_{out,1}$ can be obtained. Pierini et al. /7/ assumed a value of $x_{out,1}$ = 5 appm and a flow rate of $\dot{m}_{pu} \approx 40$ kg/s for the water cooled LiPb blanket concept /6/. For the present concept these values would result in a reduction of the tritium mass flow rate into the secondary loop to about 20 % which does not change drastically the dimensions and operating conditions of the tritium processing unit in the secondary loop. However, the tritium inventory in the primary loop increases to ≈300 g compared to 84 g. Taking into account the increased complexity of the total tritium processing system, the additional processing unit is not recommended for the given values.

If the low value of $x_{out,1}$ = 0.06 appm could be reached and high mass flow rates ($\dot{m}_{pu}$ = 2000 kg/s, compare /10/) are used, then the cold trap in the intermediate loop could be reduced to the dimensions required for the purification of other impurities. The regeneration of the cold trap to separate the tritium would be still required. However, this could happen perhaps twice a year. Again, this option would not decrease the total size and costs of the processing systems, however, is more favourable in respect to tritium inventory.

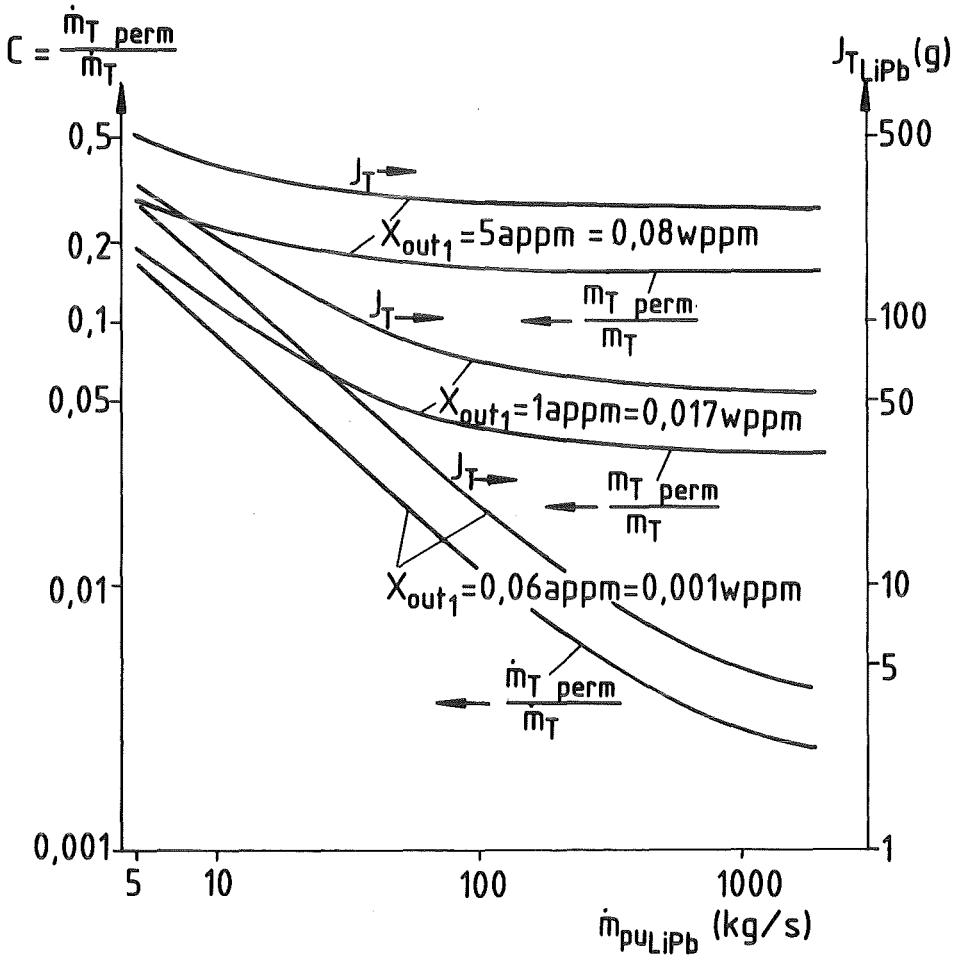

Fig. 38 Ratio of Tritium Mass Flow Rate into Secondary Loop and Tritium Inventory in Primary Loop

If the tritium inventory in the total system is to be minimized then again a ferritic intermediate heat exchanger should be chosen to reduce the tritium partial pressure in the primary loop. For a tritium inventory of about 80 g in the LiPb-loop the inlet concentration to the processing unit is then about 2 appm. A remarkable amount of tritium can only be extracted if the outlet concentration $x_{out\ 1}$ is significant lower. Presently, the achievable values fo $x_{out\ 1}$ are not known. If these values are in the range of 1 appm again the use of an additional tritium processing system is not recommended.

5.2.3 Tritum Separation by Cold Trapping in a Water-Cooled LiPb-Blanket

The inherent advantage to use the separation method discussed in this report for a self-cooled blanket with an intermediate loop was that the required area for tritium permeation into the Na or NaK loop was available due to heat transfer requirements. To use this technique for a water-cooled LiPb-blanket (compare Bioggio et. al. /6/) a permeation window is desired with a low tritium permeability to keep the tritium partial pressure in the LiPb system as low as possible.
In a previous report /10/, zirconium was discussed as permeation window for a different extraction method. This zirconium wall was covered with a palladium layer at the downstream side to catalyse tritium oxidation and to prevent oxide formation.

For the present purpose again zirconium could be considered. Again, oxide formation has to be prevented by e.g. an appropriate coating or by extensive precleaning of the small volume of the required Na or NaK by additional cold and hot trapping. Compared to zirconium, the permeability of vanadium is better known and therefore V is considered as wall material. From Fig. 39 (from Maroni and Deventer /41/) for T = 380 °C a hydrogen permeability of $Perm_H = 2.5 \cdot 10^{-3}$ $cm^3(STP)/(m \cdot s \cdot kPa^{0.5})$ is taken which corresponds to a tritium permeability of

$$Perm_T = (1/\sqrt{3})Perm_H = 1.22 \cdot 10^{-11}\ kg/(m \cdot Pa^{0.5}) \qquad (31)$$

To apply the present technique the same characteristical values as used by Pierini /7/ were assumed for the tritium concentration in the LiPb at the outlet of the permeation window, x_{out}= 5 appm = 0.0877wppm,
and for the LiPb mass flow rate $\dot{m}_{pu}$ = 43 kg/s. The temperature of the per-

meation window is T = 380 °C = 653 K. For $\dot{m}_T = 0.58 \cdot 10^{-6}$ kg/s this results in an inlet concentration of x_{in} = 0.101 wppm. The corresponding partial tritium pressures p_{T2} are calculated with Eq.(1) with K = 0.011 wppm/$\sqrt{Pa}$ and are shown in the flow diagram presented in Fig. 40.

For the cold trap circuit NaK is chosen as fluid. The cold trap mass flow rate $\dot{m}_{CT}$ is chosen to $\dot{m}_{CT}$ = 1 kg/s. The outlet concentration of the cold trap is assumed to be x_{out} = 0.192 wppm which corresponds to a saturation temperature of T_{sat} = 80 °C. To reach this outlet concentration, a cold trap temperature of T_{CT} = 50 °C is assumed, corresponding to a tritium saturation concentration of x_{sat} = 0.0366 wppm. This results in a cold trap efficiency (Eq. (7)) of 79 % which can be obtained with a residence time of about 6 min according to Fig. 12. For $\dot{m}_T = 0.58\ 10^{-6}$ kg/s and $\dot{m}_{CT}$ = 1 kg/s the inlet concentration then becomes x_{in}= 0.772 wppm. The corresponding tritium partial pressures are also shown in Fig. 40 with a value for the Sieverts constant of K = 3.15 wppm/$\sqrt{Pa}$ for T = 653 K, calculated by Eq. (2) times a factor of 3 for tritium.

To evaluate the surface of the permeation window first the concentration differences Δx_b are estimated which are required to transport the tritium by diffusion through the liquid metal boundary layers to the wall. The concentration difference Δx_b is given by

$$\dot{m}_T = A\ \rho_{\text{liquid metal}} \cdot \beta \cdot \Delta x_B \qquad (32)$$

where β is the mass transfer coefficient determined from

$$Sh = 0.023\ Re^{0.8}\ Sc^{0.33} \qquad (33)$$

with

$$Sh = \beta d/D$$
$$Re = ud/\nu$$
$$Sc = \nu/D$$

The following design for the permeation window is considered:
LiPb flows with v = 0,3 m/s inside the tubes which have an outer diameter of d = 20 mm and a thickness of s = 1 mm, the NaK flows counter currently out-

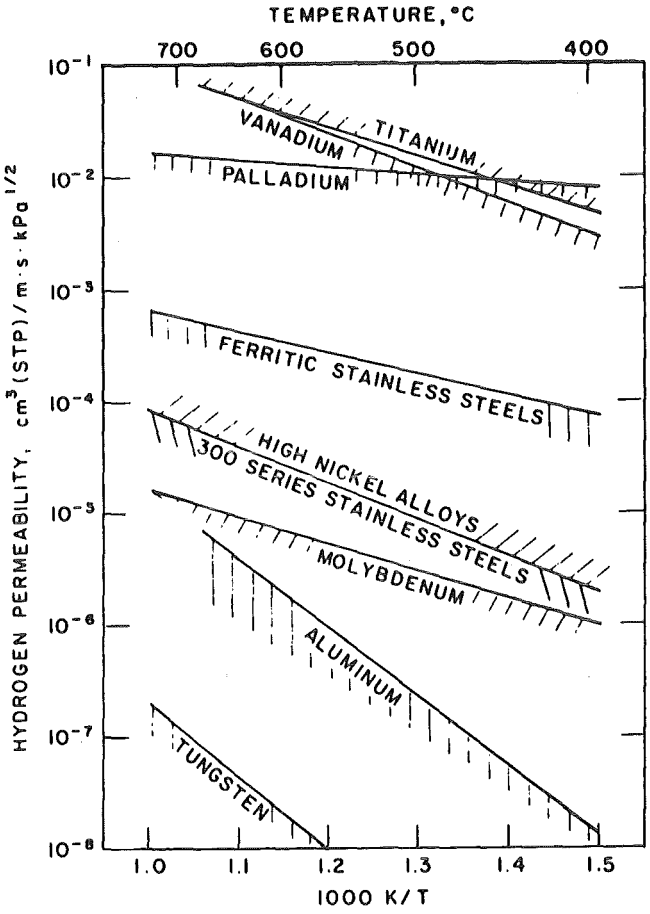

Fig. 39 Hydrogen Permeability as a Function of Temperature for Selected Metals and Alloys (from Maroni and Deventer /40/)

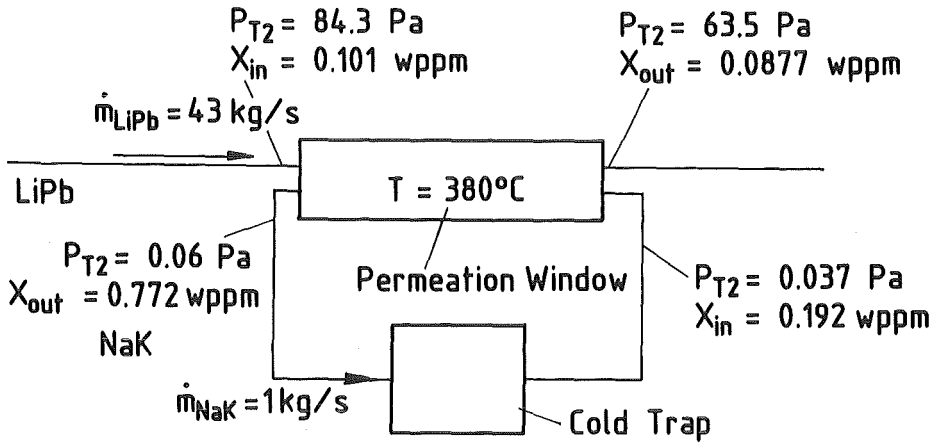

Fig. 40 Permeation Window and Cold Trap for Water Cooled LiPb Blanket

side the tubes with v = 0.106 m/s. The tube arrangement is shown in Fig. 41. For the given values the hydraulic diameter for a NaK subchannel is d = 13.6 mm.

For the given values 56 tubes are required. This tube bundle fits into a tube with an inner diameter of 0.2 m.

For LiPb, the diffusion coefficient D is assumed to D = $2 \cdot 10^{-8}$ m^2/s (/11/); the kinematic viscosity ν is calculated with the relationship given by Schulze /45/:

$$\nu = 1.9 \cdot 10^{-8} \cdot e^{1406/T(K)} \qquad (34)$$

which gives $\nu = 1.63 \cdot 10^{-7}$ m^2/s for T = 653. This results in the following values:

$$Re = 3.3 \cdot 10^4$$
$$Sc = 8.1$$
$$Sh = 189$$
$$\beta = 2.1 \cdot 10^{-4} \text{ m/s}$$

and with Eq. (32) and $\rho_{LiPb} = 9400$ kg/m^3

$$\Delta x_B(\text{wppm}) = 10^6 \cdot 0.58 \cdot 10^{-6}/(2.1 \cdot 10^{-4} \cdot 9700 \cdot A)$$
$$\Delta x_B(\text{wppm}) = 0.294/A(m^2)$$

This value corresponds to a tritium partial pressure difference of $p_{T2}(Pa) = 7.14 \cdot 10^2/A^2$.

The profile of the tritium partial pressure in the LiPb-V-NaK system is shown in Fig. 42.

For NaK, the diffusion coefficient is assumed to be the same as for Na. For T = 200 °C Hebditch /27/ gave a value of D = $6 \cdot 10^{-9}$ m^2/s. The temperature dependence of the molecular diffusivity according to Stokes law is

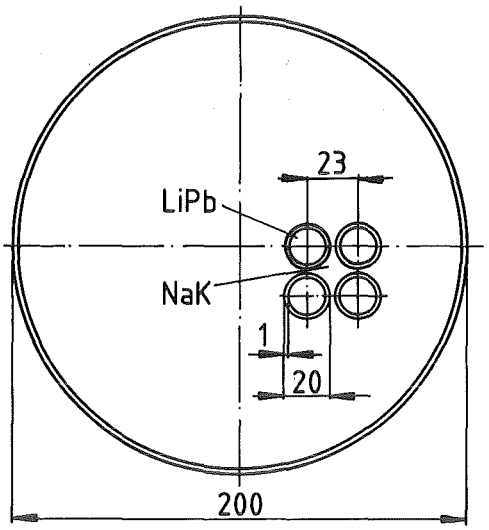

Fig. 41 Minimum Cross Section of Permeation Window

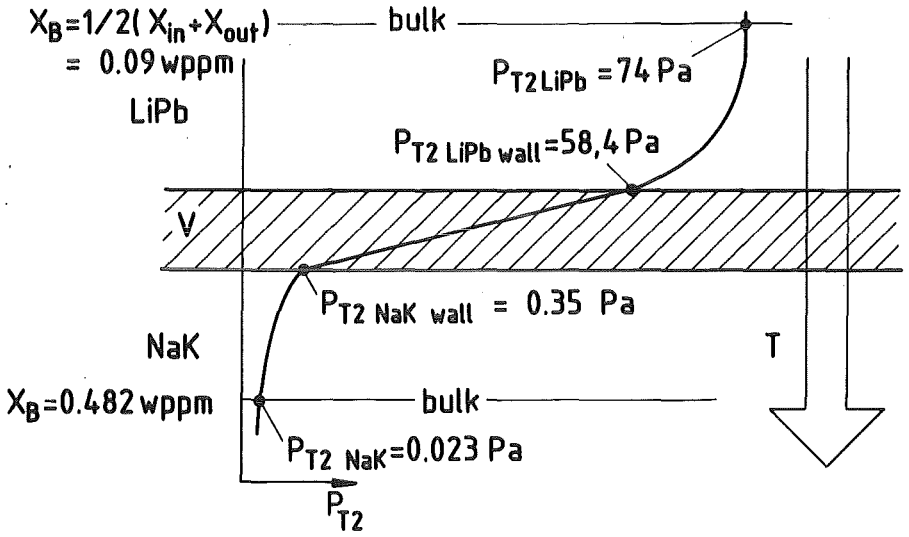

Fig. 42 Tritium Partial Pressure Profile in the LiPb-V-NaK-System

$$D \sim T/\mu(T)$$

The dynamic viscosity μ for NaK is (Bomel/Burg et. al. /46/, Fig. 1.7) μ = 0.38 centipoise at 473 K and 0.26 centipoise at 623 K. The results in D = 1.15 10^{-8} m^2/s. With $\nu = \mu/\varrho = 3.3 \cdot 10^{-7} m/s^2$ the following values are obtained:

$$Re = 4324$$
$$Sc = 28.6$$
$$Sh = 56.4$$
$$\beta = 4.77 \cdot 10^{-5} m/s$$

and finally

$$\Delta x_B(wppm) = 10^6 \cdot 0.58 \cdot 10^{-6}/(780 \cdot 4.77 \cdot 10^{-5} \cdot A)$$
$$\Delta x_B(wppm) = 15.6/A(m^2)$$

which corresponds to

$$\Delta p_{T2}(Pa) = 24.5/A^2(m^2)$$

The required permeation window surface is calculated from

$$\dot{m}_T = (A/s) \cdot Perm \cdot (\sqrt{p_{T2\ LiPb\ wall}} - \sqrt{p_{T2\ NaK\ wall}}) \qquad (35)$$

with

$$p_{T2\ LiPb\ wall} = p_{T2\ B} - \Delta p_{T2\ B} \qquad (36)$$

and

$$p_{T2\ NaK\ wall} = p_{T2\ B} + \Delta p_{T2\ B} \qquad (37)$$

The iterative solution of Eq. (35) gives A = 6.87 m^2.

With the design parameters given previously, the length l of the tube bundle becomes

$$l = A/(n \cdot \pi\ d_i) = 2.17\ m$$

The dimensions of the permeation window are pretty small even if for safety

reasons the apparatus will be built somewhat larger. The volume of the cold trap is about 0.6 m^3 which, for a cylindrical vessel, corresponds to a diameter of about 0.8 m and a height of 1.2 m. Again this apparatus is relatively small in size. Both components are very simple in design and operation compared to components required for other tritium separation methods (e.g. helium bubbling component). Therefore, this technique appears also to the attractive for a water cooled LiPb blanket.

6. Research Work to Be Done

6.1 General Aim

This chapter is an outline of research needed to provide the knowledge for a reliable design for fusion reactor blanket relevant cold traps for tritium separation and recovery. Although considerable work has been done in the field of sodium cooled fast breeders much more work is required to address the specific problems of a LiPb blanket. The following values for the main parameters are assumed:

- tritium partial pressure in the intermediate loop $p_{T2} = 10^{-2}$ Pa corresponding to tritium concentrations of $x_T = 0{,}92$ appm for Na or $x_T = 4$ appm for NaK at T = 300 °C.

- a protium partial pressure up to $p_{H2} = 10^{-1}$ Pa due to protium addition or permeation from the steam generator corresponding to $x_H = 9{,}2$ appm for Na or 40 for NaK.

- a cycle time (cold trap loading and decomposition) of up to one week.

In a first approximation, the isotopic exchange effect is neglected. Therefore, experiments using protium (in the following termed hydrogen) are proposed. As liquid metal, NaK is chosen. (However, the experimental set up should be designed such to enable easily experiments with Na).

The experimental program can be devided into three parts:
investigation of:
a) precipitation kinetics
b) precipitation morphology
c) decomposition kinetics

The experimental program (especially a) and b)) has to be accompanied by a program for model development and prediction of experiments.

6.2 Investigation of Precipitation Kinetics

The precipitation of hydrogen in NaK cold traps is to be investigated for the following parameter ranges:

hydrogen concentration	x_H = 4 - 40 appm	(≙ 0,186 - 1,86 wppm)
oxygen concentration	x_o = 0 - 5 appm	(≙ 0 - 2,39 wppm)
other impurities	x = ?	
system temperature	T = 300 - 400 °C	
cold trap temperature	T_{CT} = 30 - 100 °C	
cold trap residence times	τ = 200 - 1600 s	

The experimental cold trap (ECT) design should be very simple in order to obtain a well defined temperature distribution and to enable easily the analysis of the precipitates. A once-through design as shown schematically in Fig. 43 is recommended as used by Grundy /23/ and Latgé /26/ in similar experiments. The inner diameter is about 120 mm, the height 600 mm, resulting in a cold trap volume of about 6.8 l.

As inserts segmented mesh packings are provided whose density can vary axially. These packings are fixed on an axial rod and can be removed with the blanking plate. The NaK enters at the bottom of the cold trap and leaves at the top. The cold trap is cooled in a counter current direction by an organic fluid. To control the axial temperature distribution electrical heaters are located at the outside. Additional heaters are available for the hydride decomposition cycle. About 15 thermocouples are positioned at various locations.

For the anticipated residence times and geometry the cold trap mass flow rate $\dot{m}_T$ varies between $\dot{m}_T$ = 5,44-27 g/s corresponding to a volume flow rate $\dot{V}_{CT}$ between $\dot{V}_{CT}$ = 6,8 - 34 cm^3/s. Fig. 44 shows schematically the test loop, which is similar to the ECRIN loop described by Feron /24/. Two parallel test sections with an ECT in each case are provided. Both ECTs can be loaded simultaneously under the same conditions. The hydrogen and oxygen are fed into the system in the expansion vessel (options: injection of hydride or oxide powder, permeation of hydrogen through Ni-tubing, solution of calibrated volumns of hydrogen and oxygen gas). Prior to operation of the ECT, the hydrogen and oxygen is stored in an auxiliary cold trap. During ECT operation this cold trap in combination with a plugging meter provides constant values of the ECT inlet concentrations. The ECT inlet hydrogen and oxygen concentrations are measured with a hydrogen meter (Ni permeation type probe) and an oxygen meter (electrolytic type probe). These instruments have become much more reliable in the last years.

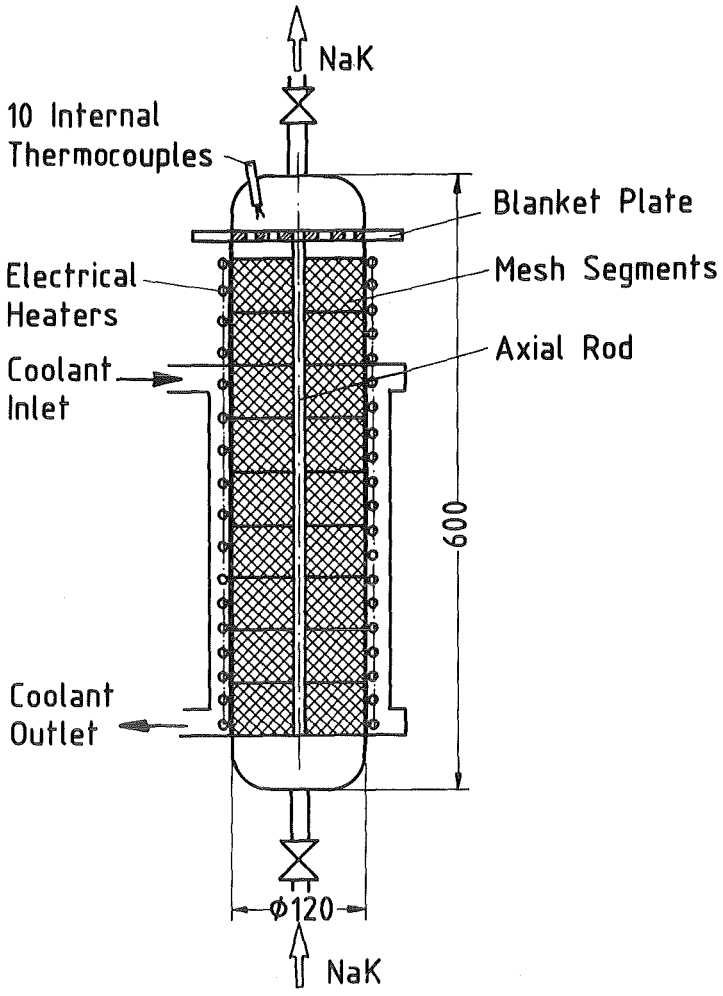

Fig. 43 Experimental Cold Trap (ECT)

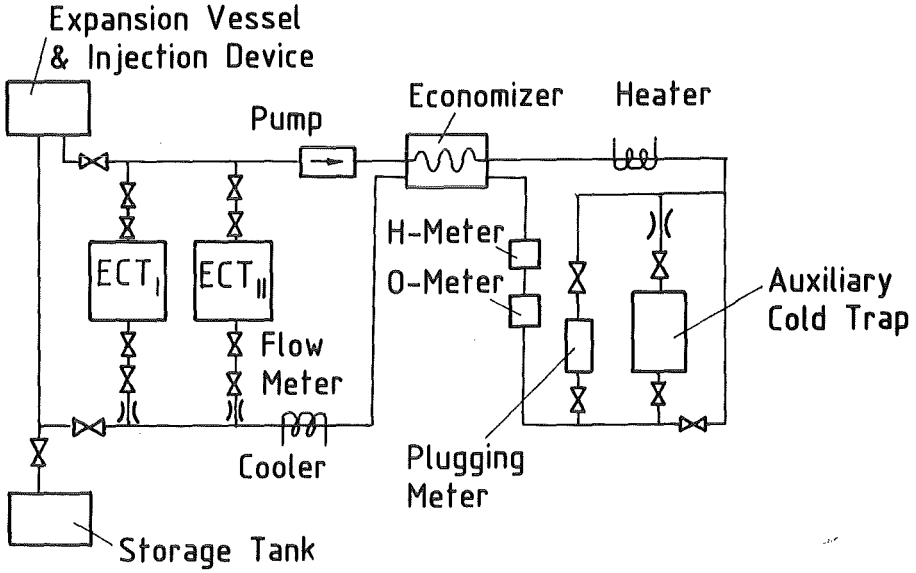

Fig. 44 Precipitation Test Loop

The experiments can be performed in a quasi-steady-state mode: after establishing an initial concentration in the circuit, the ECT starts to operate and the decline of the inlet concentration is measured (auxiliary cold trap not in operation). This method gives the cold trap efficiency as a function of time and inlet concentration, respectively, compare Fig. 11. However, the steady-state mode using the auxiliary cold trap is preferred, to load the ECT at constant inlet concentrations .

6.3 Analysis of Precipitates

Both for modeling of the precipitation and decomposition processes the following characteristics of the precipitates are of great importance:
- form of cristals, cristal surface per mesh surface
- distribution of cristals in cold trap
- composition of cristals

For this purpose the NaK in the cold trap is drained and the mesh packing is examined in a glove box in an inert gas atmosphere. Samples are taken for scanning microscopy and for quantitative chemical analysis. The hydrogen content of whole mesh segments can also be determined chemically or during the decomposition process (see chapter 6.4). If segments are no longer available for the decomposition experiments due to chemical analyses, then the second identically loaded cold trap can be used.

6.4 Investigation of the Hydride Decomposition Kinetics

The investigations on hydrogen recovery should cover the following parameter range:

- decomposition mode:	drained or undrained cold trap with vacuum pumping or inert gas bubbling
- decomposition temperature:	T_d = 300 - 450 °C
- precipitation characteristics:	form, specific surface, loading, influence of impurities (oxygen)

The technique used by McPheeters et al. /33/ is shown in Fig. 45. In the inert gas mode, the gas flow from the ECT into the reflux condenser, carrying a burden of NaK vapour and hydrogen.

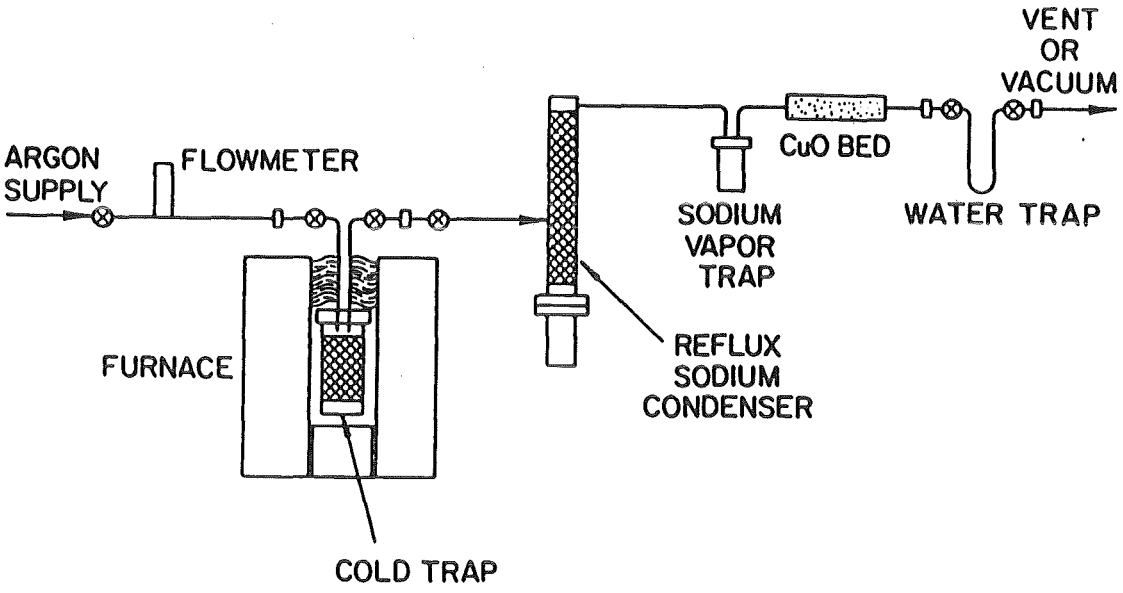

Fig. 45 Test Apparatus for Removing Hydrogen from Simulated Cold Traps (from McPheeters /33/)

Gas leaving the condenser is cooled to room temperature, enters a final vapor trap for removal of residual sodium aerosol and flows to a CuO bed that is maintained at 775 K to convert the hydrogen to water. The water vapor is collected in a trap filled with Molecular Sieve 5A adsorbent, and the quantity of water is determined by the weight gain of the trap. Two traps are used in parallel so that one trap can be weighed while the other continues to collect water. The minimum time between two measurements was about 100 s. A different measurement technique including a gas chromatograph was used by Fidler and Whittingham /29/.

When the system is operated under vacuum, the valve at the inlet to the ECT is closed and all other features of the system remain the same. The molecular sieve trap was found to retain adsorbed water under vacuum even at room temperature and with very low water loadings. Therefore, the traps were operated at room temperature during these tests /33/. Hydrogen recoveries ranging from 70 % in one experiment to > 97 % were observed.

The experimental procedure can be devided into different steps:

- In a first step the precipitated hydride is simulated by a mixture of NaH and K-H granulate, varying the particle size. These mixtures are suspended in stainless steel mesh above the bottom of the cold trap (compare /29/). From these tests the best recovery mode should be selected.
- Experiments with loaded mesh segments (from program a)) give insight in more realistic configurations and relevant parameters. In some experiments (evt. small separate effect tests), the decomposition process should be observed visually (drained cold trap). Analysis of residual impurities in the meshs after hydrogen removal have to be performed.
- A whole ECT should be used to study multiple loading and decomposition cycles. Insight could be gained on characteristical cycle times, the influence of accumulating impurities on the mass transfer processes and the corrosion behaviour.
- In further steps tritium should be used to investigate the isotopic exchange process and to conduct experiments at lower concentrations (improved measurement accuracy). These experiments are beyond the purpose of the present study and are not discussed in detail.

REFERENCES

/1/ J.S. Watson, "An Evaluation of the Methods for Recovering Tritium from the Blankets or Cooling Systems of Fusion Reactors," ORNL-TM-3794 (1972)

/2/ M.A. Abdou, et, al. "A Demonstration Tokamak Power Plant Study (DEMO)", ANL/FPP-82-1 (1982)

/3/ M.A. Abdou, et. al. "Blanket Comparison and Selection Study (BCSS), Interim Report", ANL/FPP-83-1 (1983)

/4/ D.L. Smith, et. al., "Blanket Comparison and Selection Study (Final Report)," ANL/FPP-84-1, (Sept. 1984)

/5/ D.K. Sze, "Counter Current Extraction System for Tritium Recovery from 17Li-83Pb", Sixth Topical Mtg. on The Technology of Fusion Energy, San Francisco, March 3-7 (1985)

/6/ M. Bioggio, C. Casini, F. Farfaletti-Casali, C. Ponti, M. Rieger and P.L. Bassi, "Progress in Blanket Designs with 17Li-83Pb Liquid Breeder", 13th Symp. on Fusion Technology, Varese, (Sept. 1984), Vol. 2, 1355-1364

/7/ G. Pierini, A.M. Polcaro, P.F. Ricci, and A. Viola, "Tritium Recovery from Liquid $Li_{17}Pb_{83}$ Alloy Blanket Material", Nucl. Engineering & Design/Fusion, 1 (1984), 159-165

/8/ "INTOR, International Tokamak Reactor, Phase Two A Part 1", Vienna (1983)

/9/ R.E. Buxbaum, "The Use of Zirconium-Palladium Windows for the Separation of Tritium from the Liquid Metal Breeder-Blanket of a Fusion Reactor", Sep. Science and Techn., 18 (12 & 13) (1983), 1251-1273

/10/ J. Reimann, S. Malang, private communication

/11/ K. Natesan and D.L. Smith, "Effectiveness of Tritium Removal from CTR Lithium Blankets by Cold Trapping Secondary Liquid Metals Na, K, and NaK", Nuclear Technology Vol. 22, (April 1974)

/12/ C.H. Wu and A.J. Blair, "A Study of the Interaction of Tritium with Liquid 17Li-83Pb", Proc. 12th Symp. on Fusion Technology, Julich, Germany, (September 1982)

/13/ P. Hubberstey, "Solutions of Hydrogen in Liquid Alkali Metals", Handbook of Thermodynamic and Transport Properties of Alkali Metals, Ed. R.W. Ohse, Blackwell Scientific Publications

/14/ H.W. Savage, E.L. Compere, B. Fleischer, W.R. Huntley, R.E. MacPherson, and A. Taboada, "SNAP-8 Corrosion Program, Summary Report", ORNL-3898, Oak Ridge National Laboratory (1965)

/15/ M.N. Ivanovskii, M.N. Arnol'dov, V.A. Morozov, T.I. Moiseeva, and S.S. Pleknets, Russ Metallurgy (1980), 179

/16/ R.E. Buxbaum, "A Chemical-Theory Analysis of the Solution Thermodynamics of Oxygen, Nitrogen, and Hydrogen in Lead-Rich Lithium-Lead Mixtures", J. Less Common Met. 97(1984), 27-38

/17/ K.M. Myles and F.A. Cafasso, "The Reciprocal Ternary System Na-NaOH-Na_2O-NaH", Journal of Nuclear Materials 67(1977), 249-253

/18/ H. Ullmann, "The Reactions of Oxygen and Hydrogen with Liquid Sodium - A Critical Survey", Liquid Metal Systems, Ed. H.U. Borgstedt, Plenum Press New York and London (1982)

/19/ J.D. Noden, J. British Nucl. Energy Soc. 12(1973), 329

/20/ Gmelin, "Handbuch der Anorganischen Chemie, Natrium", Chemie Verlag, Weinheim (1965)

/21/ B.R. Grundy, "On-line impurity meter responses in sodium-oxygen-third component systems", Liquid metal engineering and technology, BNES, London (1984)

/22/ M.R. Hobdell and A.C. Whittingham, "2. Reaction of hydrogen with solutions of metals in liquid sodium", Int. Conf. on Liquid Alkali Metals, Nottingham, UK, 4.-6. April (1973)

/23/ B.R. Grundy, "Experimental Characterization of Sodium Cold Traps and Modeling of Their Behavior", International Conference on Liquid Metal Technology in Energy Production, Champion. Pa., (May 1976), 650-656

/24/ D. Feron, "Etude des Mecanismes de la Purification du Sodium par les Pieges Froids", Thesis Institut National Polytechique de Toulouse, (1979)

/25/ C.C. McPheeters and D.J. Raue, "Cold Trap Modeling and Experiments on NaH Precipitation", Sec. Int. Conf. Liquid Metal Techn. in Energy Prod., Ed. J.M. Dahlke, Richland, Wash., (April 1980)

/26/ C. Latgé, "A study of sodium oxide crystallization mechanisms and kinetics in cold traps", Liquid metal engineering and technology. BNES, London (1984)

/27/ D.J. Hebditch, B.J. Gliddon, "Impurity Crystallisation in Liquid Sodium Systems", International Conference on Liquid Metal Technology in Energy Production, Champion. Pa., (May 1976)

/28/ C.C. McPheeters, D.J. Raue, "Computer analysis of sodium cold trap design and performance", Liquid metal engineering and technology. BNES, London (1984)

/29/ R.S. Fidler, A.C. Whittingham, "A comparison of alternative methods for in-situ sodium cold trap regeneration", Liquid metal engineering and technology. BNES, London (1984)

/30/ O. Winkler and R. Bakish, "Vacuum Metalurgy", Elsevier (1971)

/31/ J.R. Gwyther and A.C. Whittingham, "The Kinetics of Hydrogen Removal from Liquid Sodium", Liquid Metal Systems, Ed. H.U. Borgstedt, Plenum Press New York and London (1982)

/32/ R.S. Fidler, B.H. Targett, R. Saagi, "A study of deposition in a mesh-filled cold trap for purifying liquid sodium", Liquid metal engineering and technology. BNES, London (1984)

/33/ C.C. McPheeters, S.B. Skladzien, D.J. Raue, "Experiments on Cold-Trap Regeneration by NaH Decomposition", ANL-79-100, Argonne National Laboratory, Argonne Illinois 60439, June (1980)

/34/ C.C. McPheeters and D. Raue, "Control of Tritium in LMFBR Sodium by Cold Trapping", International Conference on Liquid Metal Technology in Energy Production, Champion, Pa., May (1976)

/35/ J. Bartlitt, personal communication

/36/ R.B. Hinze, "Chapter 1: Purification", Sodium-NaK Engineering Handbook, Vol. V, Ed. O.J. Foust, Gordon and Breach (1979)

/37/ L. Goodman, "3. The Meshless Cold Trap: A Performance Evaluation", Trans. Am. Nucl. Soc. (Jun 1978) v. 28 p. 607. ANS Annual Meeting, San Diego, CA, USA, (June 1978)

/38/ J.M. McKee, "1. Unloading Sodium Cold Traps - A Concept Exploration", 1975 ANS Annual Meeting, New Orleans, Lousiana, June 1975, Vol. 2.1, Tansao 21 1-552 (1975)

/39/ N.J.M. van Leeuwen and W.J. Westerweele, "Experiences During Testing of a Prototype Intermediate Heat Exchanger for SNR 300"; ANS Conferences; Richland, USA; April 20-24, 1980

/40/ T.A. Renner and D.J. Raue, "Tritium Permeation through Fe - 2 1/4 Cr - 1 Mo Steam Generator Material"; Nuclear Technology Vol. 22, 312 - 319 (March 1979)

/41/ V.A. Maroni and E.H. van Deventer, "Materials Considerations in Tritium Handling Systems" Journal of Nuclear Materials 85 and 86 (1979) 257 - 269

/42/ C.C. Baker et al., STARFIRE - A Commerical Tokamak Fusion Power Plant Study, ANL/FPP - 80 - 1 (Sept. 1980)

/43/ Mirror Advanced Reactor Study (MARS) UCRL-53480, (July 1984)

/44/ T. Tanabe, Y. Yamanishi, K. Sawada and S. Imoto, "Hydrogen Transport in Stainless Steels" Journal of Nuclear Materials 122 & 123 (1984) pp. 1568-1572, North-Holland, Amsterdam

/45/ B. Schulz, "Thermophysikalische Eigenschaftsmessungen am $Li_{17}Pb_{83}$ Eutektikum", Ergebnisbericht über Forschungs- und Entwicklungsarbeiten 1984 des Projekts Kernfusion, KfK 3879, (Febr. 1985)

/46/ H. Bonelbury and C. Smith, "Chapter 1: Physical Properties", Sodium-NaK Engineering Handbook, Vol. 1, Ed. O.J. Foust, Gordon and Breach, (1972)